PROTON NMR STUDIES
OF HUMAN LUMBAR INTERVERTEBRAL DISCS

Teresa Rind

B. Sc. (Physics) University of Victoria

A THESIS SUBMITTED IN PARTIAL FULFILLMENT OF

THE REQUIREMENTS FOR THE DEGREE OF

MASTER OF SCIENCE

in

THE FACULTY OF GRADUATE STUDIES

DEPARTMENT OF PHYSICS

We accept this thesis as conforming

to the required standard

THE UNIVERSITY OF BRITISH COLUMBIA

October 1990

In presenting this thesis in partial fulfilment of the requirements for an advanced degree at the University of British Columbia, I agree that the Library shall make it freely available for reference and study. I further agree that permission for extensive copying of this thesis for scholarly purposes may be granted by the head of my department or by his or her representatives. It is understood that copying or publication of this thesis for financial gain shall not be allowed without my written permission.

Department of Physics
The University of British Columbia
1956 Main Mall
Vancouver, Canada

Date: Oct. 12/90

Abstract

Problems with the low back resulting from diseases of the lumbar disc account for much human suffering and medical expense. Through early identification of changes in the disc, Magnetic Resonance Imaging offers a potential method for recognition of those at risk of low back trouble. An understanding of the chemical and structural basis of the MR image will therefore be of great help in understanding the degenerative mechanism itself. With this in mind, NMR studies of human intervertebral discs were performed to extract data that could be correlated with different stages of degeneration. *In vitro* samples of anulus fibrosus and nucleus pulposus of grades II and IV discs were examined. The Carr-Purcell-Meiboom-Gill (CPMG) pulse sequence was used to obtain T_2 relaxation data, which were analysed with a non-negative least squares algorithm and presented as a continuous spectrum of exponentials. An inversion-recovery sequence was used to obtain T_1 data which were analysed with the same algorithm, then presented as a discrete exponential spectrum. The same procedures were used to produce relaxation times from samples of isolated disc collagen and proteoglycan. Also, T_2 relaxation data were obtained with a twelve-echo CPMG imaging sequence from healthy volunteers, and these data analysed with the same procedure used for *in vitro* data.

In vivo and *in vitro* results were compared and found to agree in terms of the T_2 relaxation values. Most change between grades occurred in the nucleus, where both T_1 and T_2 values decreased from grade II to grade IV. The results of the proteoglycan and collagen studies support the theory that structure, not chemical composition, is responsible for the observed changes in relaxation times. Based on estimates of the percentages of protons in the nucleus due to water, proteoglycan and collagen, tentative

assignments were made to the components of the T_2 spectra for grades II and IV nucleus, and these were supported by the results of all parts of the study.

Acknowledgements

I would first like to thank my supervisor Alex MacKay, who made this project possible. He provided guidance and encouragement, and shared his expert knowledge of the workings of the Room 100 magnet and spectrometer. He also set up and developed the partnership with Richard Pearce's group in the UBC Department of Pathology, found many valuable reference papers, offered advice on this thesis, and obtained all of the MRI CPMG data.

I enjoyed working with Dick Pearce, Joyce Mathieson, and Gwen Bebault from the Department of Pathology at the UBC Hospital, and greatly appreciate all the time and thought they contributed. Specifically, I would like to thank Dick for sharing his extensive knowledge of the intervertebral disc and offering suggestions on the direction of the project, as well as providing all of the samples and many valuable reference papers. I would also like to thank Joyce who prepared *in vitro* disc samples and taught me how to prepare the collagen and proteoglycan samples; and Gwen who shared thoughtful insights on the study of degenerative discs.

The crew in Room 100 have been very supportive and provided help in solving day-to-day problems with the equipment and computing system. Thanks to Clare Morrison, our system manager, the computing system in the lab has been running well and has enabled me to do experimental work and writing without interruption. Also, the relaxation results would not have been possible without Ken Whittall's NNLS program.

Finally, I would like to thank Julia Wallace for showing me the ropes in Room 100.

Table of Contents

Abstract ii

Acknowledgements iv

List of Tables vii

List of Figures viii

1 Introduction 1

2 The Intervertebral Disc 3

2.1 Composition of the Disc 5

2.2 Disc Degeneration 7

2.3 Disc Grading Scheme 9

3 Proton NMR Theory 12

3.1 Basic NMR and Relaxation Theory 12

3.2 NMR of Water in Biological Samples 17

4 Application of NMR to Intervertebral Discs 23

4.1 Advantages of Magnetic Resonance 23

4.2 Purpose of This Work 24

5 Experimental Methods 25

5.1 Experiments Performed 25

5.2 Sample Preparation 27
5.3 Data Collection 27
5.3.1 T_2 and the CPMG Sequence 28
5.3.2 T_1 and the Inversion Recovery Sequence 29
5.3.3 In Vivo CPMG 30
5.4 Data Analysis 30
5.4.1 Analysis of CPMG Data 31
5.4.2 Analysis of Inversion-Recovery Data 32

6 Results **37**
6.1 T_2 and T_1 of Disc Samples 37
6.2 In Vivo MRI T_2 Values 46
6.3 Solid Signal in Disc Samples 51
6.4 T_1 and T_2 of Collagen Samples 51
6.5 T_1 and T_2 of Proteoglycan Samples 53

7 Discussion **55**

Bibliography **61**

List of Tables

5.1 Disc Samples 26

5.2 Collagen Samples 26

5.3 Proteoglycan Samples 26

6.1 T_2 Values for Nucleus and Anulus of Disc Samples 38

6.2 T_1 Values for Nucleus and Anulus of Disc Samples 38

6.3 Average T_2 Values for Grades II and IV Anulus and Nucleus 40

6.4 Average T_1 Values for Grades II and IV Anulus and Nucleus 41

6.5 T_2 Values of In Vivo MRI Samples 46

6.6 Average In Vivo T_2 Values for Each Lumbar Disc 47

6.7 T_1 and T_2 Values for Collagen Samples 53

6.8 T_1 and T_2 Values for Proteoglycan Samples 53

7.1 Tentative Assignments to the T_2 Spectrum 59

List of Figures

2.1 The Lumbar Spine and The Intervertebral Discs 4

2.2 Components of the Disc 4

2.3 Disc Grading System by Morphology and MRI 10

5.1 Examples of Discrete and Continuous NNLS Spectra 34

5.2 NNLS Spectra With Different Values of Facmu 35

5.3 Example of NNLS Fit to CPMG Data 36

6.1 Typical T_2 Spectra for In Vitro Disc Samples 39

6.2 T_2 Values for In Vitro Disc Samples — Nucleus 42

6.3 T_2 Values for In Vitro Disc Samples — Anulus 43

6.4 T_1 Values for In Vitro Disc Samples — Nucleus 44

6.5 T_1 Values for In Vitro Disc Samples — Anulus 45

6.6 T_2 Values for In Vivo MRI Samples 48

6.7 Graph of Mean MRI T_2 Values for Each Disc 49

6.8 Histogram of T_2 Values for MRI Samples 50

6.9 Solid Signal in Disc Samples 52

6.10 Proteoglycan T_1 and T_2 Relaxation Rates Versus Concentration 54

Chapter 1

Introduction

Problems with the spinal column in humans are widespread, costly, and serious. Sixty to eighty percent of all adults have experienced back pain at some time in their lives, with most of these symptoms occurring in the lower portion of the spine, the lumbar region. The most common disorders giving rise to the pain are instability and misalignment, disc degeneration, spinal stenosis, and facet disease. Accompanying the pain are sensory changes and weakness in the body. The social impact of these phenomena is striking when one considers that back trouble leads to many worker's compensation claims, time lost from work, and great hospital costs. In fact, degenerative disorders of the spine are the leading cause of disability in the working years; over any twelve month period approximately 25% of working men will have back trouble. In addition, these disorders are among the most common causes of impairment in general, and account for a major portion of medical expenses. [1,2]

Most scientists believe that lower back pain is often due to disc degeneration, as alterations in disc structure may cause pain and impairment by affecting nerves and the spinal cord. Extensive research has been conducted in the epidemiology, anatomy, biomechanics, biochemistry and neuromechanics of the disc and spine, but the pathophysiology of disc degeneration and the role of biochemical changes are poorly understood, and complex. Autopsy results show that by the fifth decade of life, 85–95% of the population have degenerate discs. Possible contributing factors to disc degeneration are thought to be genetic makeup and biomechanics. Indeed, disc failure occurs in the

areas of the spine that undergo the most mechanical stress; the role of genetics is not so easy to observe or define. [1,2,3]

What *is* known is that degeneration begins early in life and occurs in everyone, to different extents among individuals [2,4]. A method of early detection of problem discs would help in preventing unnecessary injury and pain; a better understanding of the causes and mechanisms of disc degeneration would be the first step in finding an effective prevention and/or cure. Magnetic resonance may be the solution to both of these needs. MRI could be used to non-invasively detect early degenerate discs, and knowledge of the theory behind the images could lead to an understanding of the degenerative process.

Chapter 2

The Intervertebral Disc

Intervertebral discs play a remarkable role in stabilizing the spine by anchoring the vertebrae to one another, allowing a fair amount of movement of the spine, absorbing loads, and always regaining their original size and shape. Discs vary in size, from the smallest cervical discs in the neck region, to the largest lumbar discs in the lower back (Figure 2.1). They contain special types of cartilage which are noted for their strength and resilience. The tensile strength comes from collagen fibrils, and the resilience is due to large proteins called proteoglycans. In this type of tissue, it is the extracellular material that is important, rather than the cells themselves. In fact, the disc is mostly water and extracellular matrix, including some of the largest proteins made by any cell in the body. [3,5]

The body of a healthy disc is composed of two distinct regions: the inner gelatinous *nucleus pulposus* surrounded and contained by the fibrous rings of the *anulus fibrosus*. Outside the disc body are the cartilage endplates and vertebral bodies, as illustrated in Figure 2.2.

The nucleus pulposus (NP) is a proteoglycan-rich matrix interspersed with a relatively small number of randomly oriented collagen fibres. Cell density in this region is only 4000 cells/mm^3, being mostly chondrocytic and fibroblastic in type, with a smaller number of notochordal cells. [1,3]

The anulus fibrosus (AF) is made up of 15–20 concentric layers of collagen fibres, organized so that the fibres of adjacent laminae are at 40–90° to one another. The cells

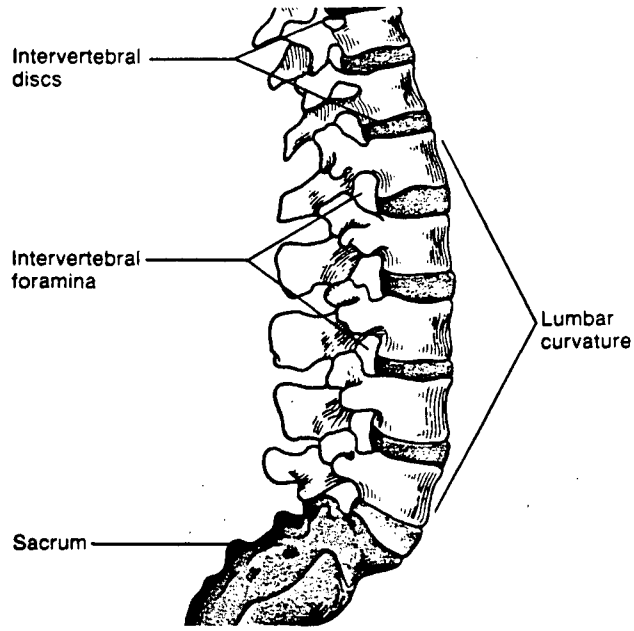

Figure 2.1: **The lumbar spine and the intervertebral discs.** This drawing of the lumbar spine shows the positioning of the intervertebral discs between the vertebrae. (From Human Anatomy by K. M. Van De Graaff, Wm. C. Brown Publishers, Iowa, 1988. p171.)

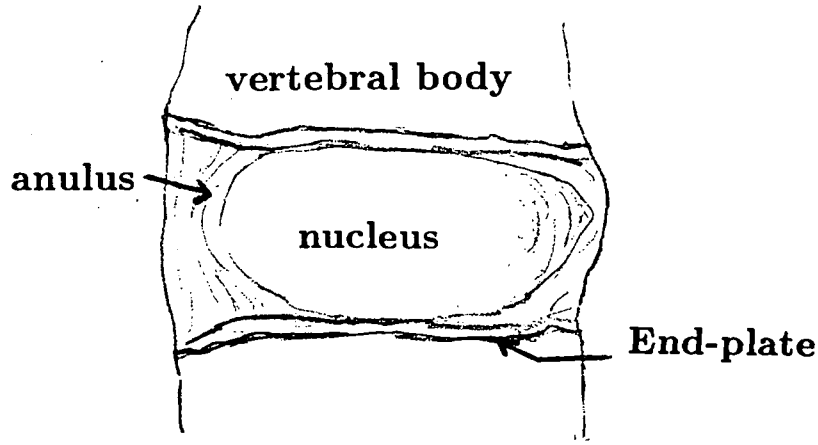

Figure 2.2: **The components of the healthy intervertbral disc.** The drawing illustrates the anulus fibrosus, nucleus pulposus, endplates and surrounding vertebral bodies.

of the outer anulus are fibrocytic while the inner cells are chondrocytic. [1,3]

Nutrient transport in the disc is unique, due to the fact that only the outermost layers contain blood vessels, lymphatics and nerves. In fact, discs are the largest volumes of tissue in the body without nerves and vessels. Nutrients reach the cells in the disc by moving through the matrix from the blood vessels at the edges. Some transport is achieved by entrainment in moving fluid under changing loads, and another means is active transport by chondrocytes, but the main mode of nutrient travel through the matrix is diffusion. Thus, the maximum concentration of any nutrient or solute in the matrix may be controlled by the local proteoglycan content. [3,5,6]

2.1 Composition of the Disc

Collagen Collagen is found throughout the disc, in various fibril concentration, diameter, and organization. Ten types of collagen have been found in the disc, with types I and II being the most abundant, followed by type VI. Type I, found mostly in the anulus, increases from 0–80% abundance towards the outer layers, while type II collagen increases 0–80% in the opposite direction, being found mostly in the nucleus. Type VI is found in both regions, 10% in the AF and 15–20% in the NP. In adult lumbar discs, the dry mass in the outer anulus fibrosus is 60–70% collagen, and 10–20% collagen in the nucleus pulposus. As far as structure goes, the fibrils in the outer anulus are arranged in tight concentric layers at angles to one another; the inner anulus fibrils are less dense and less organized; and in the nucleus they form a loose network with no organization. [2,3]

The general structure of a collagen fibril starts with procollagen, the precursor. This is a protein with about 1100 amino acids, every third one being glycine and one third of the others being proline or hydroxyproline. The procollagen molecule twists into

a compact left-handed helix; three of these form a right-handed superhelix, a rod-like macromolecule approximately 1.4 nm in diameter and about 300 nm long. Groups of these superhelixes form the fibrils, which are from 10 to 200 nm in diameter, and of varyied length. They possess great tensile strength as a result of the multiple twisting and grouping. [5]

Proteoglycan Like collagen, proteoglycans are present throughout the disc. They are similar to the proteoglycans of articular cartilage in many ways, but differ in several respects that may be important in the degenerative process. [1]

Different regions of the disc contain one or more of five distinct species of proteoglycans, though the relationships amongst these species are not yet defined. One population of disc proteoglycans form large macromolecular aggregates while the rest do not, and the proportions of these two groups differ between anulus and nucleus. Their relative amounts also change with aging: some elaborate PG aggregates are found in newborns' discs but not in mature spines. Another grouping of the proteoglycans is in terms of their components. One family is rich in keratan sulfate while another contains large amounts of chondroitin-6 sulfate. These repeating disaccharides are two of the main constituents of proteoglycans in general, as described below. [3,7,8,9]

The central molecule of a proteoglycan is the repeating disaccharide hyaluronic acid, to which are attached amino acid chains called core proteins. The attachment is achieved without chemical bonding, by use of a link protein and a good fit with a globular shape formed from the end of the core protein. Each core protein then has many polysaccharide chains attached to it. Three regions are defined on the core protein by virtue of what is attached: (1) the linkage region containing the globular end and a few small sugar chains; (2) a region having keratan sulfate chains and small o-linked oligosaccharides; and (3) a region with chondroitin sulfate chains. There are

approximately 50 keratan sulfate chains and 100 chondroitin sulfate chains on a core protein, and there may be up to 100 core proteins on a central strand of hyaluronic acid when large aggregates form. The overall weight of such an aggregate may be many tens of millions of atomic units. [5,6]

Water Acting with collagen and proteoglycans to give discs their unique properties is water, which makes up about 70% of the healthy disc. The repeating disaccharides chondroitin sulfate and keratan sulfate contain sugars which carry negative charges, forming a large ordered array of electronegativity. Since water is a dipole, H_2O molecules become organised in layers around these proteoglycan charges. When the disc is under pressure from loading, the water is forced away from the negative charges and they become closer together. Electrostatic repulsion prevents further compression; as soon as the load is reduced the H_2O returns to its former arrangement and the structure is restored. Thus water plays a major role alongside proteoglycans in providing the disc with resilience. The movement of fluids also helps to nourish the tissue as explained in Section 2. [3,5]

While a proteoglycan molecule can structure an amount of water many times its own weight, this is not the only way H_2O is stored in the disc: some is trapped in the interstices of the proteoglycan and collagen matrix. The structured water, however, is reponsible for the important disc properties. [5]

2.2 Disc Degeneration

As the disc ages or degenerates, structural and chemical changes occur affecting all components of the tissue. As the disc becomes more fibrous and disorganised, the distinction between anulus and nucleus becomes less clear. All collagen fibrils increase in diameter and more chondrocytic cells appear, while proteoglycan and water content

decrease. Water loss runs to 30%, with the majority lost from the nucleus. Disc volume can shrink dramatically, in some cases from 15 cc to 1 cc, causing secondary effects from increased forces at the facet joint, such as misalignment, arthritic changes and potential fractures. [1,2,3,4]

Some of the water loss is related to changes in the proteoglycan molecules; a decrease in the molecular weight of proteoglycan aggregates in the nucleus leads to a decrease in water-structuring capacity. Not only do the aggregates lose size, but there are fewer of them, and the remaining proteoglycans become smaller. The small scale chemical structures of the proteoglycans do not change, but the relative amounts of the components do. For example, the ratio of chondroitin sulfate to keratan sulfate increases in some parts of the disc and decreases in others. Also, a diminished association with collagen results in some loss of tensile strength. [2,3]

Data seem to indicate that proteoglycan is lost from all discs of a spine before any morphologically recognizable degeneration takes place. This loss of proteoglycan is thought by some to stem from a long term decrease in nutrient supply. This may be partly due to the fact that less vessels penetrate the anulus as the disc ages. It may also be related to an accumulation of large macromolecular fragments which the disc cannot remove, resulting in abnormal biomechanical and biophysical tissue properties. The cellular feedback mechanism would become confused and the matrix would not function properly or maintain itself. This is one possible explanation of degeneration. [1,3,4,8]

The extracellular matrix does seem to have a limited ability for resynthesis and repair, though it is not known if the repair is good enough to restore long term function. Most restructuring occurs in the anulus with the collagenous material being resynthesized most easily; repair in the nucleus is minimal. [3]

One of the main problems in finding an explanation for disc degeneration is that the relationships have not been well defined between age-related changes in the disc and the development of clinical syndromes or change in function. Normal aging and abnormal degeneration are difficult to separate. [3]

2.3 Disc Grading Scheme

A disc grading scheme has been devised by J. P. Thompson and associates [3, page 193] [10,11] for assessment by gross morphology and Magnetic Resonance Imaging. The scheme delineates five stages of degeneration based upon the appearance of mid-sagittal sections of the lumbar disc. Features affecting the classification are the nucleus pulposus, anulus fibrosus, cartilaginous and bony end-plates, and the periphery of the vertebral body. Figure 2.3 illustrates the appearances of the five grades by morphology and MRI.

Grade I discs (found in the young) are identified by a bulging gel nucleus, a distinct fibrous anulus with discrete layers of collagenous fibres, and a uniformly thick hyaline endplate. In the MR T_2-weighted spin echo image with TE = 90 ms, the nucleus appears uniformly bright and the anulus uniformly dark grey, with the endplate appearing as a single dark line.

Grade II discs (the healther discs examined in this project) still have a bulging nucleus with gel at its centre, but white fibrous tissue appears around the edges, and the anulus contains mucinous material between the fibrous laminae. The endplate is no longer uniform in thickness. MRI shows some loss of brightness in the central horizontal plane of the nucleus in the form of dark bands, and light areas in the anulus.

The infiltration of fibrous tissue into the nucleus and the invasion of mucinous material into the anulus increase through grades III and IV, with the clear demarcation

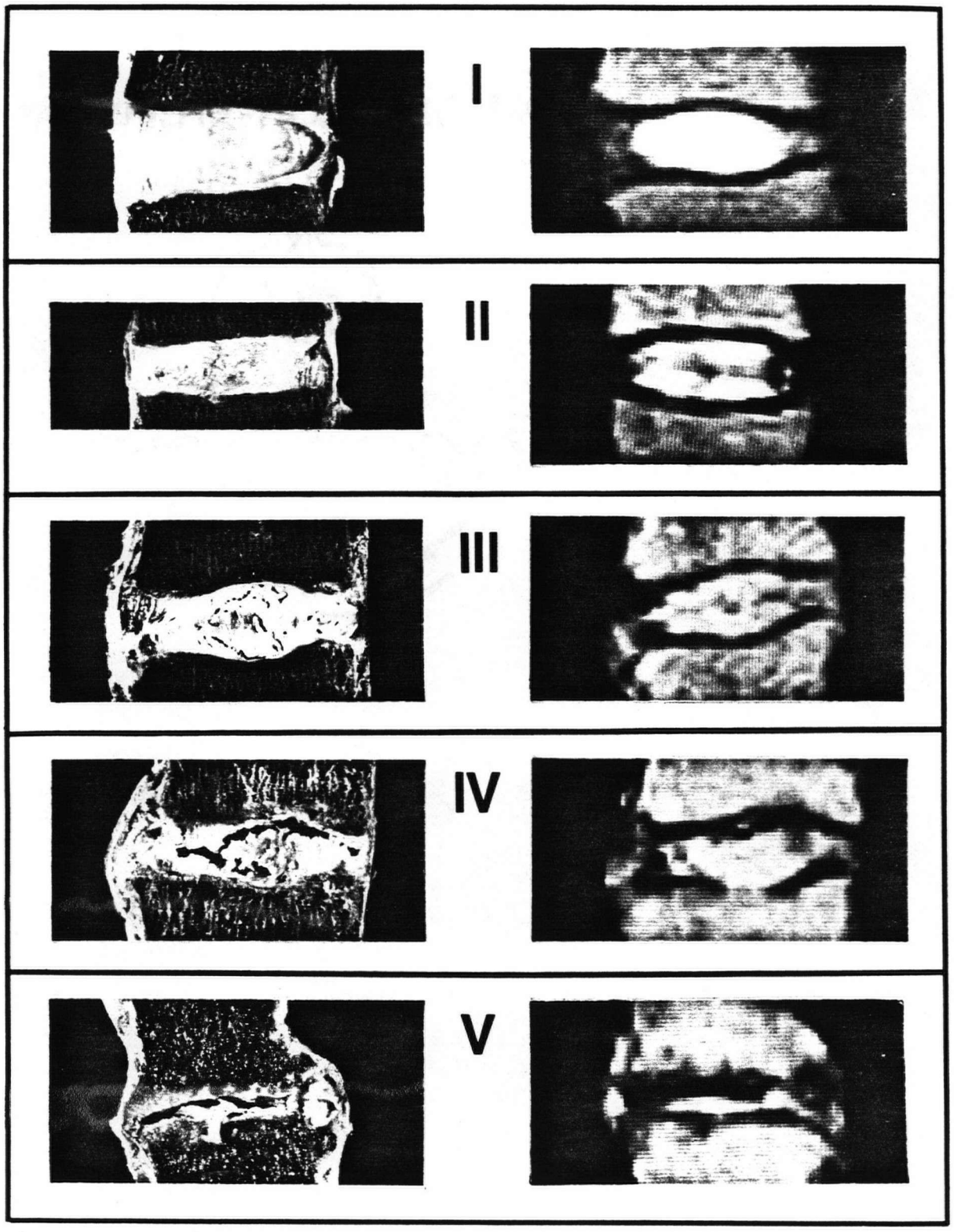

Figure 2.3: **The morphologic and MRI grading system.** Photographs of actual disc slices are shown at left, and MR images of corresponding grade are shown at right. (Courtesy of R. H. Pearce)

between nucleus and anulus dissolving at the grade III level. In a grade IV nucleus there are also horizontal clefts parallel to the endplate, and the anulus contains focal disruptions. In the MR image the nucleus and anulus are indistinguishable, with increasing regions of bright and dark signal and decreasing grey areas. Focal defects appear in the line of the endplate in the grade IV disc.

Finally, the grade V disc is severely degenerate, with clefts extending through the remaining tissue (nucleus and anulus are indistinguishable), and diffuse sclerosis in the endplate. The MR image reveals defects and thick areas in the endplate, extreme loss of overall disc height, and dominant bright and dark signals in the disc body.

Chapter 3

Proton NMR Theory

A brief overview of basic NMR theory leading to the T_1 and T_2 relaxation processes is contained in the following section, which has been summarized from C. P. Slichter's Principles of Magnetic Resonance [12]. For more details please refer to this source.

The second part of this section describes briefly some relevant aspects of the NMR of water in biological tissues, including water structuring, proton transfer, cross-relaxation, and compartmentation.

3.1 Basic NMR and Relaxation Theory

A nucleus has total magnetic moment $\vec{\mu}$ and total angular momentum $\vec{J}$ related by

$$\vec{\mu} = \gamma \vec{J} \tag{3.1}$$

Define a dimensionless operator $\vec{I}$ such that $\vec{J} = \hbar \vec{I}$ and it follows that

$$(Im|\mu_{x'}|Im') = \gamma\hbar(Im|I_{x'}|Im')$$

where m and m' are spin quantum numbers. If one applies a field $\vec{H}$, the interaction energy of the nucleus will be $-\vec{\mu} \cdot \vec{H}$. The Hamiltonian is thus

$$\mathcal{H} = -\vec{\mu} \cdot \vec{H}$$

Taking the field to be H_0 along the z-direction gives a Hamiltonian of

$$\mathcal{H} = -\gamma\hbar H_0 I_z$$

The eigenvalues are thus multiples of the eigenvalues of I_z: for $I = 1/2$, we have

$$E = -\gamma\hbar H_0 m, \quad m = -1/2, \ +1/2$$

To detect these energy levels, one needs an interaction that causes transitions between these levels, i.e. one needs

$$\Delta E = \hbar\omega$$

where ω is an angular frequency. In NMR one uses an alternating magnetic field applied perpendicular to a static field H_0. The perturbing term in the Hamiltonian is

$$\mathcal{H}_{pert} = -\gamma\hbar H_x^0 I_x \cos\omega t$$

where H_x^0 is the amplitude of the alternating field and ω is the frequency of that field.

I_x has matrix elements between states m and m' which disappear unless $m' = m \pm 1$. Allowed transitions are between adjacent levels:

$$\hbar\omega = \Delta E = \gamma\hbar H_0$$

so that

$$\omega = \gamma H_0$$

Thus we can find ω needed to observe a resonance, if we know γ. To estimate γ, a classical picture is used, by computing the magnetic moment and angular momentum of a charged particle moving in a circular path. Then by comparing the expressions for μ and J and considering equation 3.1, we get $\gamma = e/2mc$, where e is the charge of the particle, m is the mass, and c is the speed of light. A general result of this is that large masses have low γ's. For magnetic fields around 2 Tesla, hydrogen nuclei (protons) resonate at about 90 MHz.

Spin-Lattice Relaxation: Consider nuclei of spin 1/2, each with two states, $m = +1/2,\ -1/2$, called $|+\rangle$ and $|-\rangle$. Some nuclei will be in the $|+\rangle$ state, and some in the $|-\rangle$ state at a given time. Call the number in the $|+\rangle$ state N_+, and the number in the $|-\rangle$ state N_-.

To see that there must usually be a coupling of the spins to another system (the lattice), consider the magnetization of an unmagnetized piece of material: a net number of transitions from upper to lower state is required, so the spins give up energy, which is accepted by another system, a reservoir (the "lattice").

Let $W\uparrow$ be the probability per second that the coupling will induce a spin transition from $|+\rangle$ to $|-\rangle$ (higher energy) and let $W\downarrow$ be the probability for the reverse process. $W\uparrow$ and $W\downarrow$ are unequal, seen by considering what is happening in the coupled system (Slichter, page 8). Then if n is defined as $N_+ - N_-$, the population difference, and N is the total population, using

$$\frac{dN_+}{dt} = N_- W\downarrow - N_+ W\uparrow$$

we get

$$\frac{dn}{dt} = \frac{n_0 - n}{T_1} \tag{3.2}$$

where

$$n_0 = N\left(\frac{W\downarrow - W\uparrow}{W\downarrow + W\uparrow}\right)$$

and

$$\frac{1}{T_1} = (W\downarrow + W\uparrow)$$

The solution is

$$n = n_0 + Ae^{-t/T_1}$$

where A is a constant of integration, n_0 is the population difference at thermal equilibrium, and T_1 is a characteristic time related to the approach to equilibrium. T_1 is called the "spin-lattice relaxation time".

Effect of Alternating Field $\mathbf{H_1(t)}$: An alternating field can be considered as two rotating components of equal amplitude, rotating in opposite directions. One rotates in the same sense as the precession of the spins, but the other, going the opposite way, will not be "seen" by the spins. A spin sees only $H_1(t) = H_1(\hat{\imath}\cos\omega_z t + \hat{\jmath}\sin\omega_z t)$. The equation of motion for a spin in fields $\vec{H}_0$ and $\vec{H}_1(t)$ is

$$\frac{d\vec{\mu}}{dt} = \vec{\mu} \times \gamma \left[\vec{H}_0 + \vec{H}_1(t)\right]$$

One can eliminate the time dependence by working in a rotating coordinate system (rotating about the z-axis with frequency ω_z). Then both H_0 and H_1 will be time independent. If we set up the x-axis along H_1, we have

$$\frac{\delta\vec{\mu}}{\delta t} = \vec{\mu} \times \left[\hat{k}(\omega_z + \gamma H_0) + \hat{\imath}\gamma H_1\right]$$

Near resonance, $\omega_z + \gamma H_0 \approx 0$ (set $\omega_z = -\omega = -\gamma H_0$). The above equation can also be written as

$$\frac{\delta\vec{\mu}}{\delta t} = \vec{\mu} \times \gamma\vec{H}_{eff}$$

where

$$\vec{H}_{eff} = \hat{k}\,(H_0 - \omega/\gamma) + \hat{\imath}H_1$$

So in the rotating system, the moment will precess in a cone about $\vec{H}_{eff}$ at angular frequency γH_{eff}. At exact resonance ($\omega = \gamma H_0$) we have $\vec{H}_{eff} = H_1\hat{\imath}$, and $\vec{\mu}$ will precess in the y-z plane. Application of H_1 then for a time t_p (applying a "pulse") will cause the moment to precess through an angle

$$\theta = \gamma H_1\, t_p$$

One can choose H_1 and t_p to produce any angle θ; for example, a "180° pulse" is when $\theta = \pi$.

Thus to put spins into the x-y laboratory plane, one must apply a ninety degree pulse ($\theta = \pi/2$); in the lab frame, spins will then precess about the z-direction. This is detected through an induced emf in the same coil used to apply the pulse.

Interactions of spins with each other and with the lattice cause decay of the signal (emf) detectable in the x-y plane. This decay is called the "Free Induction Decay" (free of H_1) and may be exponential in nature, though this is not generally the case.

Bloch Equations for Free Induction Decay: Knowing that $M_z = \gamma\hbar n/2$ and using equation 3.2, one expects that

$$\frac{dM_z}{dt} = \frac{M_0 - M_z}{T_1}$$

where M_0 is the magnetization at thermal equilibrium.

Also, the x and y components of the magnetization are reduced over time due to spin-spin interactions, and this decay is represented by the following equations:

$$\frac{dM_x}{dt} = -\frac{M_x}{T_2}$$
$$\frac{dM_y}{dt} = -\frac{M_y}{T_2}$$

where T_2 is introduced as a different relaxation time than T_1. This is because while the longitudinal (T_1) decay involves a change of energy (transferred to the lattice), the transverse decay conserves energy. The exponential form of the transverse decay is arbitrary but is useful to describe some important phenomena. It is important to note that the processes causing T_2 relaxation are *irreversible* processes.

Spin Echoes: For liquids, whose T_2 values are on the order of tenths of a second or seconds, inhomogeneities in the $\vec{H}_0$ field can dephase spins at a rate higher than the transverse relaxation rate, thus "covering up" the real T_2 value which one wants to observe. To eliminate the effect of the magnet inhomogeneity, *spin echoes* are used.

A spin echo is created by applying a 90° pulse to put the magnetization into the x-y plane, followed by a 180° pulse a time τ afterwards. Before the 180° pulse, the spins will have dephased due to the inhomogeneities; some will be "ahead" and some will be "behind", by the angle

$$\theta = \gamma \delta H \tau$$

where $\delta H = H - H_0$, the difference in local field from H_0. After the 180° pulse, the spins that were ahead will now be behind, and vice versa, so that after another time τ they will line up again. At this time, 2τ from the initial 90° pulse, a spin echo will be observed as an isolated peak in the detected transverse magnetization amplitude. Note that during the period 2τ the effects of T_2 relaxation will continue unaffected by the 180° pulse, so that the amplitude of the echo signal will be

$$M(2\tau) = M_0 e^{-2\tau/T_2}$$

for single exponential relaxation behaviour.

3.2 NMR of Water in Biological Samples

Most or all of an NMR or MRI signal from a biological sample is due to protons of water, so understanding the behaviour of this water is vital to any analysis of relaxation results. Some signal may come from the proton-rich solutes which are a source of relaxation events, but this is fairly insignificant compared to the contribution of water protons. [15]

States of Water in Tissues: Water in biological tissues behaves differently from bulk water, in that it is structured around macromolecules as described in Section 2.1. A small fraction of the H_2O molecules interact with slow-moving constituents such

as proteins and cell walls via electrostatic interactions and hydrogen bonding, forming a well-defined hydration layer in solutions, hydrated fibres such as collagen, and all biological samples such as intracellular H_2O and tissues. The hydration layer is characterized by water molecules that are oriented and restricted in motion, thus with different properties from bulk water. [13,14]

Most fat-free tissues can be considered to contain three water fractions, based on their location and behaviour: *bound* water consists of H_2O molecules hydrogen-bonded to fixed sites on macromolecules; *structured* water is motionally perturbed by the macromolecules but not bonded to them; and *bulk* water's motion is solely determined by the interactions between H_2O molecules. Each fraction has its own relaxation rates, governed by the motion of the molecules, proton transfer processes, and spin exchange. [15]

Interactions between H_2O and macromolecules: The most important source of relaxation time shortening in tissues is due to changes in the motion of water molecules near the macromolecular surface. This restricted motion in the hydration layer is not uniform, leading to anisotropic diffusion of H_2O molecules. Macromolecules with different protein content also have different water-perturbing capacities, so the behaviour of hydration water depends strongly on the nature of the hydrated species. [13,15]

Magnetic dipole-dipole coupling is the important interaction in proton water studies, and this is affected by molecular motions such as rotation, which varies the orientation of local fields, and translation. Magnetic interactions are partially averaged by the rotations, and when water molecules diffuse through regions of different orientations. Averaging also occurs when proton transfer takes place, and this process is enhanced along a continuous hydrogen-bonded path in the hydration layer of a macromolecule. [13,15]

Relaxation rates in tissues: True T_2 decay is caused by random dephasing of the x-y magnetization due to rapid molecular tumbling motion and the resulting changing magnetic field. There is also a contribution to T_2 caused by dephasing from a "static" component of the magnetic coupling between proton pairs: large macromolecules rotate slowly on the NMR timescale, appearing to be motionless from the NMR point of view. The relatively short T_2 in tissues is partly a result of this static dephasing. [15]

In general, tissue relaxation rates are affected by: (1) the strength of local magnetic interactions between nuclei, (2) molecular motion (anisotropic rotation and translation), (3) water perturbing capabilities of the macromolecules, (4) proton transfer rates, (5) diffusion rates, (6) water content, and (7) spin exchange or cross-relaxation rates [13,15]. The first three items affect intrinsic relaxation rates, while the remaining four characteristics affect the observed rates, which may differ from the intrinsic rates. *Compartmentation* is based on the assumption that sites of different relaxation characteristics exist and the protons at these sites interact with each other in various ways [14,15]. For example, the protons of different sites may be exchanged (proton transfer) or water molecules from one compartment may diffuse to other regions with different local relaxation rates. Water content affects the observed relaxation rates by determining the ratio of bulk water to structured water, both of which have different intrinsic rates. Restricted water motion near the macromolecules gives the structured water a smaller T_2 value [13]. When water content decreases and a larger proportion of water is structured, the observed T_2 value is shortened.

Cross-relaxation (spin exchange): Cross-relaxation between protein and solvent protons also makes an important contribution to the relaxation rates of hydration water. Spin exchange occurs when the motion of protons from the hydration layer and protons from macromolecules is correlated. Under this condition, there will be a

mutual exchange of spin magnetization between these protons. When $T_2 \ll T_1$ and slow molecular diffusion is present, energy exchanges much faster within the system of spins than between the spin system and the lattice. Note that since the motion of macromolecules depends upon the molecular weight and shape, and cross-relaxation in turn depends on the motion of the macromolecules, then relaxation times of protein solutions are related to the size and shape of the proteins. There may also be cross-relaxation arising from rotations of components of the macromolecule. [13,15]

An example of cross-relaxation is seen in studies of collagen, where a short T_1 component is seen due to spin exchange between water and proteins. To determine this, inversion pulses of various lengths were used in a T_1 experiment. The short T_2 of collagen causes dephasing of the spins during the pulse, so the longer the pulse, the less protons in the protein are inverted. This means there are also more "solid" protons with which water protons must share their reservoir of excited spins. After equilibrium is reached between the water and protein protons, the slope of the decay is the true average T_1 of the solution; the slope of the initial steep decay curve gives information about the spin exchange rate. This is known as intermolecular cross-relaxation. [15]

Fast and slow exchange: If the spin exchange rates of water protons between different areas in a sample are fast compared with the instrinsic relaxation rates ("fast exchange"), then an average water resonance signal is seen. If, on the other hand, the exchange rate is relatively slow ("slow exchange"), then a resonance signal characteristic of water protons in each site may be seen. [13]

Under conditions of fast exchange between two regions, the observed T_1 value will be:

$$\left(\frac{1}{T_1}\right)_{obs} = X_f\left(\frac{1}{T_{1f}}\right) + X_h\left(\frac{1}{T_{1h}}\right)$$

where X_f is the fraction of free or bulk water, X_h is the fraction of hydration water, and

T_{1f}, T_{1h} are the spin-lattice relaxation rates of free and hydration water, respectively [13]. In soft tissue, the observed relaxation rate is thus the weighted average of all components within a diffusion radius of a water molecule [15].

Slow exchange occurs often in fatty tissues, where the lack of hydrogen-bonding sites limits cross-relaxation between water and fat. In this case the two compartments relax separately. [15]

Compartmentation: When a tissue is compartmented, T_2 is shorter than T_1 and shorter than T_2 of bulk water, and is often multiexponential in nature [14]. There is, however, disagreement over the number of H_2O compartments and the relaxation characteristics of each compartment. A continuous model has been proposed, but often three compartments are sufficient to describe the relaxation behaviour of biological systems. [14,15]

The fact that in compartmented systems T_1 is usually single exponential and T_2 is multi-exponential is explained via the rates of exchange processes between compartments: the rates are fast on a T_1 timescale but slow on a T_2 timescale. This is not a universally accepted theory, however, and other explanations have been proposed, such as a diffusion dominated process where the distance to an interface (between compartments) cannot be traversed within the intrinsic relaxation time of the diffusing species, so one observes a variety of relaxation times. [14]

This view is presented by Brownstein and Tarr [16], who assume that all relaxation is due to magnetization sinks either contained within an active volume or on an active surface to which the molecule must diffuse. The general solution is:

$$\mathcal{M}(t) = \sum_{n=0}^{\infty} I_n \exp(-t/T_{j,n})$$

where $\mathcal{M}(t)$ is the appropriate magnetization at time t, I_n is the intensity of the n^{th}

component, and $j = 1, 2$. Only the first two or three terms are important for systems with only active surfaces (cell walls, for example). The T_1's, T_2's and I's depend on the local geometry, diffusion coefficient, and the strength of the relaxation sink. This model is best applied to systems with compartments on the order of micrometres across containing localized sinks such as walls, though there may be many other systems yet to be studied where this model fits. [14,16]

Chapter 4

Application of NMR to Intervertebral Discs

4.1 Advantages of Magnetic Resonance

The main problem of studying intervertebral discs is inaccessibility. Many techniques for gleaning information about the disc do not provide enough data or are insensitive to changes within the disc body, while others are invasive and risky to the patient. Magnetic Resonance Imaging possesses none of these problems and is now the "state of the art" technique for examining discs. The reasons are obvious when the abilities of this method are weighed against those of plain film radiography, myelography, contrast discography and computed tomography. [1,3]

Plain film radiography shows advanced changes only, such as disc space narrowing, endplate sclerosis, and osteophyte formation, but does not reveal changes in the disc itself. Myelography only shows bulging of the disc, herniation, and spinal stenosis. Discography is invasive, dangerous, and controversial, and computed tomography is insensitive to changes that occur before the onset of structural changes. [1]

On the other hand, MRI gives soft tissue contrast, excellent spatial resolution, and provides multiplanar imaging. The anulus and nucleus can be distinguished, unlike with any of the other techniques. The latest surface coil technology, cardiac gating, gradient refocussing and contrast agents have allowed for much enhancement of these features. [1,2]

Most importantly, MRI is very sensitive to early changes in the disc, reflecting the

structural and chemical changes of degeneration. The signal appears to be correlated with proteoglycan content and distribution, and seems to reflect these attributes even better than gross morphology; this will help enormously with the investigation of the exact relationship between proteoglycan content and degeneration. [1,3]

The role of magnetic resonance could go to actual tissue characterization of biochemical change and pathology. An early example of this sort of application is a study of the so-called "hamburger effect", where a low-intensity horizontal strip is seen in the middle of the nucleus in T_2-weighted mid-sagittal images. Chemical breakdowns of the regions of different signal intensities showed no disparity in chemical concentrations, suggesting that tissue distribution and structure are responsible for the effect, not chemical composition. Further studies will investigate the relationship between tissue structure and T_2 values to find out what is different about the "hamburger" region. Through this type of work a full understanding of the degenerative mechanism and its causes may be possible. [1,2]

4.2 Purpose of This Work

The objective of this work is to take the first step in attempting to relate the degenerative changes described in Section 2.2 to the magnetic resonance image of the disc. This would lead to a possible understanding of the degenerative mechanism and also make MRI a reliable diagnostic tool for many types of back trouble. The first step is to obtain a base of NMR data from discs in different stages of degeneration, from which initial inferences can be made and general trends can be observed.

This project focuses on the discs of the lumbar spine, where most trouble occurs.

Chapter 5

Experimental Methods

5.1 Experiments Performed

The main portion of this study involved the examination of anulus and nucleus *in vitro* samples from two MRI grades of disc: II and IV. From six discs, both anulus and nucleus were studied, while from another five discs only the nuclei were used. This was decided after little difference was found between the results from the two grades of anulus. For the first six disc samples, $T_1$and T_2 data were collected, as well as the free induction decays; for the five nucleus samples only T_2 values were found, as this became the focus of the study. The ratio of solid to liquid signal was also obtained for nucleus and anulus. Table 5.1 lists all the disc samples and their statistics.

In a parallel experiment, *in vivo* T_2 data were collected by MRI from the discs of volunteers aged 20–70 years with no history of back problems, in conjunction with a study by Pearce and Flak [1]. All lumbar disc nuclei (L1–L2 to L5–S1) were examined for 19 volunteers.

Some analysis of disc tissue components was also carried out in the hopes of obtaining more insight into the origins of the T_2 data. Two partly denatured collagen samples from grades II and IV discs were analysed for T_1 and T_2 values, compared and contrasted (Table 5.2). Proteoglycan also was examined from anulus and nucleus in three different concentrations in saline solution (Table 5.3).

Table 5.1: Disc Samples

Sample	Spine #	Disc	Grade	AF	NP
HD1	C16	L5–S1	II	√	√
HD2	U36	L5–S1	IV	√	√
HD3	C13	L3–L4	II	√	√
HD4	C14	L5–S1	IV	√	√
HD5	C23	L5–S1	II	√	√
HD6	C25	L5–S1	IV	√	√
HD7	C28	L2–L3	II		√
HD8	C18	L5–S1	IV		√
HD9	C27	L1–L2	II		√
HD10	C30	L1–L2	IV		√
HD12	C30	L2–L3	IV		√

Table 5.2: Collagen Samples

Sample	Spine #	Disc	Grade	AF	NP
C1	C16	L3–L4	II	√	√
C2	U36	L2–L3	IV	√	√

Table 5.3: Proteoglycan Samples

Sample	AF/NP	Proteoglycan Dry Wt. (mg)	Amount of Solution (ml)	Concentration (mg/ml)
PGN1	NP	20.4	0.1314	155.3
PGN2	NP	20.4	0.2756	74.0
PGN3	NP	20.4	0.4093	49.8
PGA1	AF	14.1	0.0982	143.6
PGA2	AF	14.1	0.1970	71.6
PGA3	AF	14.1	0.2815	50.1

5.2 Sample Preparation

For the grades II and IV disc study, lumbar discs from a number of spines were dissected by Pearce et al. [1] to obtain samples of anulus and nucleus about 0.2 cc, small enough to fit into an 8 mm diameter NMR tube. The spines had been obtained within 24 hours of death and kept frozen at −80°C. The NMR samples were kept frozen, and thawed to room temperature only for the data collection period. Consistent results were found for those samples refrozen, then rethawed for repeat data collection, so this method of storage was assumed to be appropriate.

For the collagen samples, intervertebral disc collagen (remaining after extraction of proteoglycan with 4M guanidinium chloride) was washed four times with a solution of phosphate buffered saline (pH 7.4) and soaked overnight. The residue left after the final centrifuge was placed in an NMR tube and kept frozen, until data collection at room temperature.

The proteoglycan was dissolved in the saline solution at initial concentrations of 155 mg/ml and 143 mg/ml for the nucleus and anulus proteoglycan, respectively. Subsequent lower concentrations were achieved by adding further amounts of saline solution to the same samples after data collection. Samples were kept refrigerated while in storage.

5.3 Data Collection

Data were collected on a custom-built data acquisition system comprised of a Nicolet Explorer Digital Oscilloscope, DB32016 slave computer (National Semiconductor Corporation), modified Bruker SXP–100 Spectrometer, custom pulse programmer, custom interface board, and the main computer, a DEC MicroVAX. The configuration was

[1] UBC Department of Pathology

designed and put together by E. Sternin. [17]

Samples in 8mm NMR tubes were placed inside the probe of a 2.0 Tesla electromagnet, tuned at 90 MHz for water. Magnet inhomogeneity was reduced as much as possible by shimming.

The images for the MRI *(in vivo)* data were collected on the 0.15 Tesla whole body imager at the UBC Hospital.

5.3.1 T_2 and the CPMG Sequence

T_2 data were obtained with the Carr-Purcell-Meiboom-Gill pulse sequence which uses the concept of spin echoes described in section 3.1. The basic sequence is the following:

$$90^\circ_x - \tau/2 - 180^\circ_y - \tau - 180^\circ_y - \tau - \cdots$$

Each scan consisted of two CPMG pulse trains, first the above sequence, then the following:

$$90^\circ_{-x} - \tau/2 - 180^\circ_y - \tau - 180^\circ_y - \tau - \cdots$$

which produces a negative signal, after which the two data sets are subtracted to cancel out coherent noise and baseline offset. One hundred scans were performed and averaged to give good signal-to-noise.

Tau values used in this case were 200, 400 and 800μs, to check for any tau dependence. Early results showed none, so only 200 and 400μs were used in subsequent data collection. At each spin echo between 180° pulses, four data points were collected in the vicinity of the echo peak, to be averaged later. To get an optimal representation of both fast and slow decay rates, every echo was recorded for the first 224 echoes, then every eighth echo out of the next 4096, after which the remaining FID was collected on a free-running time base. Baseline was also collected before the sequence, for 1400μs.

The details of the data point collection are as follows:

$$90^\circ_x - \tau/2 - 180^\circ_y - 37\tau/80 - \text{collect } 1\mu\text{s} -$$
$$\left[(\frac{\tau}{40} - 1\mu\text{s}) - \text{collect } 1\mu\text{s}\right] \times 3 - 35\tau/80 - 180^\circ_y - \cdots$$

Ninety degree pulse lengths were set so that two in succession were equal to one 180° pulse, rather than just halving the determined 180° length. This avoided errors due to the rounding of the pulse edges, which would cause a pulse whose length was half of a 180° to be less than 90°. (The longer the 180° pulse, the closer the 90° will be to half the duration.)

Actual pulse lengths used ranged from 5.5μs to 7.8μs for a 180° pulse, varying from week to week as the available rf power varied.

5.3.2 T_1 and the Inversion Recovery Sequence

The spin-lattice (T_1) relaxation data were collected using the following inversion-recovery sequence:

$$-(\text{trigger scope}) - 50\mu\text{s baseline} - 90^\circ_x - \text{collect} - 10\text{s recovery}$$
$$180^\circ_x - \tau - (\text{trigger scope}) - 50\mu\text{s baseline} - 90^\circ_x - \text{collect} - 10\text{s recovery}$$

The amplitude of the signal right after the ninety degree pulse in the second portion of the sequence should be proportional to $(1 - 2e^{-(\tau+50\mu s)/T_1})$, accounting for T_1 effects only. To eliminate effects of variations with time, a single 90°_x pulse was first applied to record the original longitudinal magnetization amplitude, then the inversion-recovery sequence was performed and that data subtracted from the single 90°_x data. One can see that complete inversion recovery would yield a zero signal after subtraction. In other words, this sequence found the difference in longitudinal magnetization from before the 180° pulse to a time τ' afterwards, which is $2M_z(\tau{=}0)e^{-\tau'/T_1}$ where $\tau' = \tau + 50\mu s$.

One hundred scans were taken for each τ value, and eleven different τ values were

used, logarithmically covering an extensive time period:

$$1ms, 5, 10, 20, 100, 500, 1000, 2000, 3000, 4000, 5000ms$$

180° pulse lengths were the same as for the CPMG sequence. Signal from both the x and y channels was collected so that any phase offset could be set to zero later by data manipulation.

5.3.3 In Vivo CPMG

A twelve-echo imaging sequence was written for *in vivo* MRI by A. MacKay, with 20 ms echo spacing (τ), four averages per echo, and TR = 2000 ms. The sequence was applied to a single 10 mm sagittal midline slice, with the 30 cm field of view broken down into a 128 × 256 matrix of signal intensities for each echo image.

Using a DEC PDP 11/34 graphics package with a RAMTEK image analysis system, a trackball was used to highlight the nucleus of each disc in the first echo image; then the average signal intensity, standard deviation, and total area were recorded for each of the twelve images, calculated from the same region of interest each time. Signal intensities were then written to VAX/VMS files, listed opposite their corresponding echo times, ready for T_2 analysis.

5.4 Data Analysis

Several pre-written and some new Fortran 77 programs were utilized on the MicroVAX system for analysis of the data in various states. CPMG analysis programs were written by A. MacKay[1], K. Whittall[2], and H. Le, and T_1 data handling routines were written by A. MacKay. New programs written for this project were designed to facilitate handling of results output by the other programs.

[1]Physics, [2]Geophysics and Astronomy Depts, UBC.

5.4.1 Analysis of CPMG Data

The raw *in vitro* CPMG data were converted to a more useful form by the program CPMGANL2, written by A. MacKay and H. Le. This program averaged the four points for each echo, calculated the corresponding echo times, subtracted baseline, and took only the top 99% of the signal. From the baseline the noise was estimated with a standard deviation calculation. The output consisted of a list of positive echo amplitudes and their corresponding times, as well as the number of echoes and the standard deviation of the baseline.

To assign T_2 values using this form of the data, a non-negative least squares (NNLS) program written by K. Whittall [18] was applied to produce a spectrum of T_2 values using linear inverse theory. The echo amplitude was fitted with a series of exponentials in the form

$$S(t) = \sum_{i=1}^{N} A_i \exp(-t/T_{2i})$$

where $S(t)$ is the fitted signal amplitude at time t, N is the number of exponentials used in the fit (120 in this project), A_i is the weighting factor for the i^{th} component, and T_{2i} is the i^{th} T_2 value in the spectrum. A discrete or continuous fit could be chosen. A set of N T_2 times was created prior to running the program, logarithmically covering a range wide enough to include all possible transverse relaxation times for the materials being studied. For the disc samples, a scale from 10^{-3}s to 10^{0}s was adequate, while a wider range of times (to 10s) was needed for the proteoglycan and collagen samples.

Examples of both discrete and continuous fits are shown in Figure 5.1. The continuous fit was chosen for all T_2 analysis as this gave unambiguous results. For this type of fit, an adjustable parameter called "facmu" controlled the amount of curvature allowed in the spectrum by weighting the first derivative. The smaller the value of facmu, the less defined were the spectrum peaks, and vice versa. Figure 5.2 illustrates the effect

of changing facmu from 100 to 500. In the study, facmu was chosen so that each peak in the spectrum was distinct, if not separated, from its neighbours. An indication of this was the symmetry of a peak; i.e., how close the weighted average T_2 value was to the value with the largest amplitude (at the top of the peak). T_2 results quoted in this report are the weighted average values, though as stated above these were very close to the maximum amplitude values.

The goodness of fit was indicated by the χ^2 value calculated by the NNLS program. A good fit should have χ^2 close to the number of degrees of freedom (n_f); i.e. in this case the number of points being fit. This number depended on the number of echoes in the top 99% of the signal, and this number fell within the range 90–190. The value of χ^2 depended greatly on the estimated noise, or baseline standard deviation. In most cases, χ^2/n_f fell between 0.9 and 1.2, while sometimes just one or two errant points in the early data could be enough to blow up χ^2 . Fit to the data was checked by plotting the fit along with the data points, and this always showed an excellent match (Figure 5.3). Changing facmu did not alter χ^2 dramatically.

5.4.2 Analysis of Inversion-Recovery Data

The raw T_1 data was transformed into an array of values $(M(0) - M(\tau))$ versus τ, by a program written by A. MacKay. For each of the eleven different τ value data sets, the program subtracted the baseline and output the average intensity for a data window following the 90° pulse. A noise estimator was also calculated from the baselines of all eleven data sets, by finding their standard deviation.

With the inversion-recovery data represented as a decreasing function of time (in the form $2M_z(\tau{=}0)e^{-\tau/T_1}$) they could be analysed with the NNLS program in a similar procedure to the T_2 analysis. For the T_1 data, however, the relaxation was nearly single exponential, and the discrete fit was chosen with no ambiguity of results. This

allowed for easy extraction of the T_1 value by looking at the spectrum, and without the bother of adjusting facmu. The T_1 time scale for the 120 exponential fit covered the range 10^{-3}s to 10^{1}s. The χ^2 goodness of fit was expected to be near 11 (the number of degrees of freedom) but was often much lower due to overestimation of noise. Plotting the calculated data with the actual data showed an excellent fit as in the case of T_2 analysis.

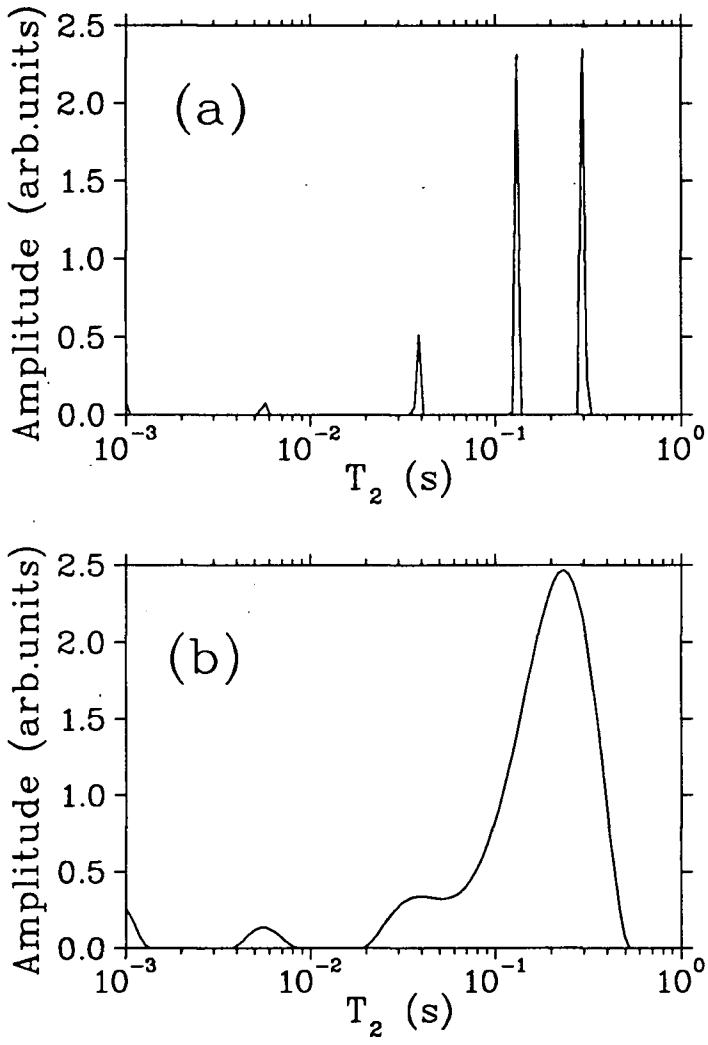

Figure 5.1: **Examples of NNLS spectra, fitted to CPMG data.** (a) A discrete spectrum. (b) A continuous spectrum. The continuous spectrum has less ambiguity for multiexponential relaxation, and does not differ between data sets from the same sample.

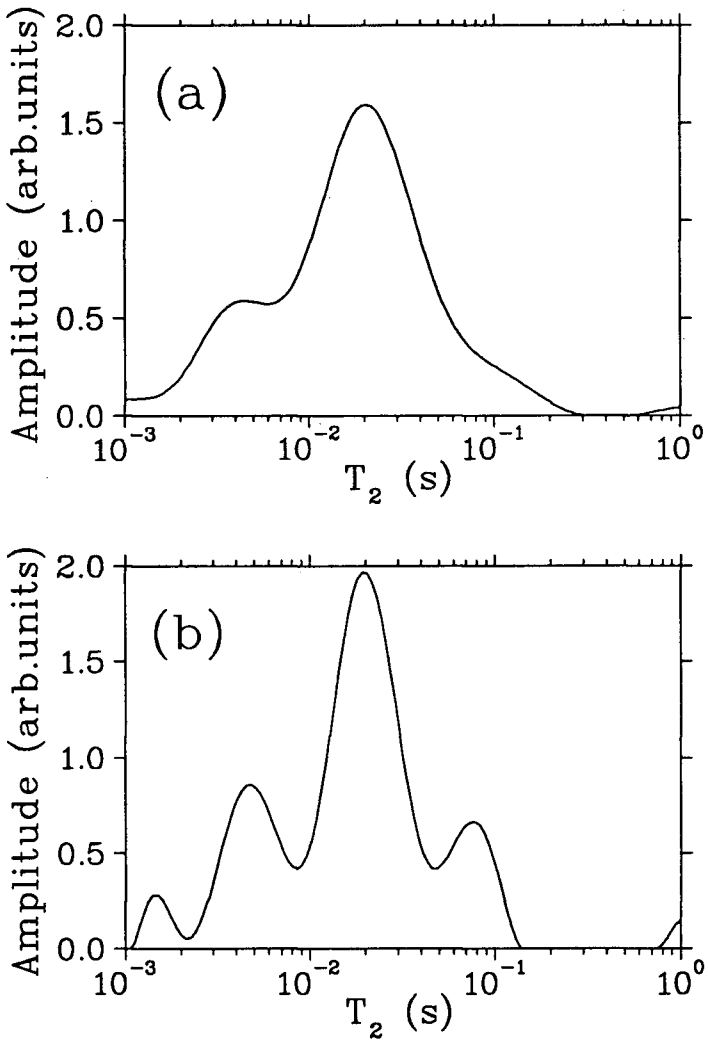

Figure 5.2: **The effect of changing facmu on an NNLS continuous spectrum.**
(a) Facmu=100. (b) Facmu=500. Facmu is a variable parameter that controls the amount of curvature allowed in the spectrum, by weighting the first derivative. More peaks are visible and each one is narrower when facmu is larger.

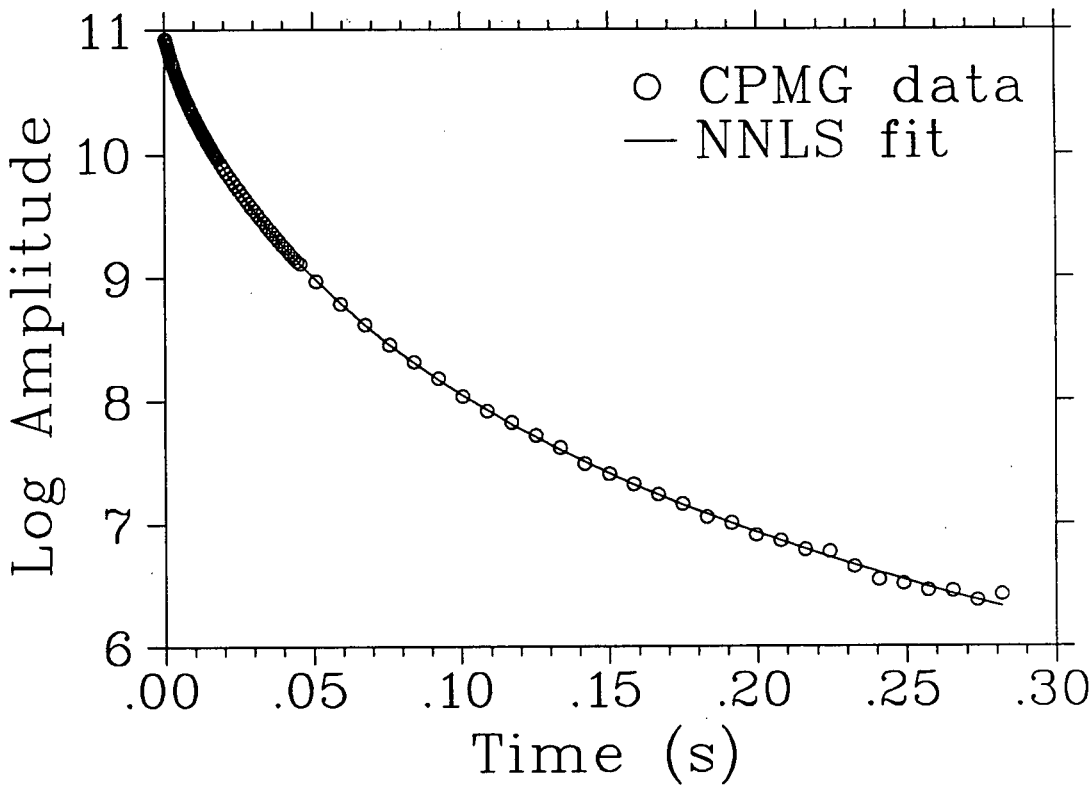

Figure 5.3: **A plot of an NNLS fit to CPMG data.**
The actual data are shown as "o" symbols and the calculated signal is a solid line; the two are a close match.

Chapter 6

Results

6.1 T_2 and T_1 of Disc Samples

Table 6.1 lists all the T_2 values and their percent contributions to the continous spectra obtained for the nucleus pulposus and anulus fibrosus samples of grades II and IV discs. With the exception of HD8N, results for $\tau = 200\mu s$ and $\tau = 400\mu s$ were very close, so both tau value results are shown for HD8N. Some typical T_2 spectra are also shown in Figure 6.1 to illustrate the origin of the results in Table 6.1. All T_1 results are summarized in Table 6.2, which lists the components of the discrete spectra and their percent contributions.

Figures 6.2–6.5 are plots of the results in Tables 6.1 and 6.2, with the dominant contributions (above 20%) shown as solid symbols and the lesser components as empty symbols. For the case of HD8N, the tau value whose fitted χ^2/n_f was closest to one was chosen for plotting in Figure 6.2.

T_2 — Nucleus Pulposus: Figure 6.2 clearly shows a difference in T_2 values between grade II and grade IV nucleus samples. The dominant contributions (solid symbols) for grade II mostly lie above 100 ms while the T_2 values for grade IV fall in the range 20–70 ms. The only overlap is from sample 5 where there are two components over 20%, the lesser one (31%) at 55 ms and the larger one (49%) at 156 ms; and sample 9, where there are two components over 20% also, the smaller at 220 ms and the larger at 69 ms. Sample 9 was also the one for which the $\tau = 200\mu s$ and $\tau = 400\mu s$ results

Table 6.1: **T_2 Values for Nucleus and Anulus of Disc Samples**

#.Sample	AF/NP	Grade	T_2 Values (ms) and % Contributions			
1. HD1N	NP	II	5.5 (2%)	36 (8%)	105 (23%)	255 (67%)
2. HD3N	NP	II	6.4 (4%)	38 (12%)	101 (84%)	
3. HD5N	NP	II	4.6 (2%)	20 (5%)	101 (93%)	
4. HD7N	NP	II	2.5 (1%)	15 (4%)	156 (95%)	
5. HD9N	NP	II	4.5 (5%)	15 (15%)	55 (31%)	156 (49%)
6. HD2N	NP	IV	3.6 (8%)	23 (92%)		
7. HD4N	NP	IV	2.4 (2%)	12 (7%)	47 (90%)	498 (1%)
8. HD6N	NP	IV		9 (2%)	42 (96%)	247 (1%)
9. HD8N[a]	NP	IV	1.7 (2%)	18 (9%)	69 (52%)	220 (37%)
9. HD8N[a]	NP	IV		9 (5%)	104 (95%)	
10. HD10N	NP	IV	5.4 (2%)		49 (98%)	
11. HD12N	NP	IV	4.8 (2%)		49 (98%)	
1. HD1A	AF	II	2.9 (14%)	13 (51%)	43 (33%)	392 (2%)
2. HD3A	AF	II	4.0 (12%)	15 (41%)	38 (47%)	
3. HD5A	AF	II	2.9 (22%)	10 (52%)	29 (26%)	
4. HD2A	AF	IV	1.7 (1%)	11 (6%)	64 (91%)	562 (2%)
5. HD4A	AF	IV	3.5 (22%)	12 (57%)	39 (21%)	
6. HD6A	AF	IV	4.8 (10%)	22 (90%)		

[a]HD8N is the only sample for which CPMG results from the two different tau values did not agree, so both are shown here, in order of increasing τ.

Table 6.2: **T_1 Values for Nucleus and Anulus of Disc Samples**

#.Sample	AF/NP	Grade	T_1 Values (s) and % Contributions	
1. HD1N	NP	II	0.62 (2%)	1.4 (98%)
2. HD3N	NP	II	0.69 (34%)	1.5 (66%)
3. HD5N	NP	II	0.25 (5%)	1.6 (95%)
4. HD2N	NP	IV	0.64 (100%)	
5. HD4N	NP	IV	0.83 (89%)	1.2 (11%)
6. HD6N	NP	IV	0.75 (98%)	3.5 (2%)
1. HD1A	AF	II	0.69 (83%)	1.3 (17%)
2. HD3A	AF	II	0.47 (51%)	1.2 (49%)
3. HD5A	AF	II	0.70 (93%)	1.4 (7%)
4. HD2A	AF	IV	1.10 (92%)	1.9 (8%)
5. HD4A	AF	IV	0.78 (95%)	1.5 (5%)
6. HD6A	AF	IV	0.69 (100%)	

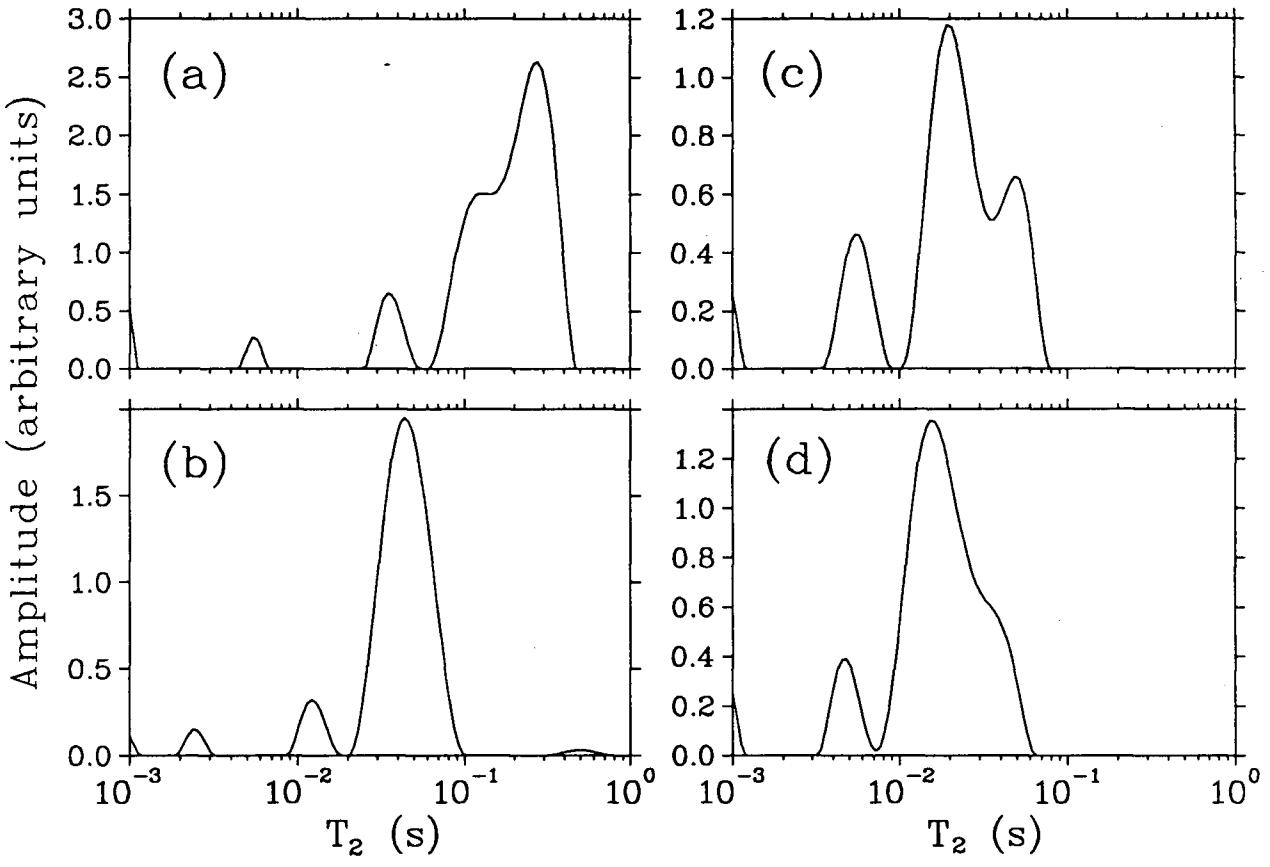

Figure 6.1: **Typical T_2 spectra for in vitro disc samples.**
(a) Grade II nucleus. (b) Grade IV nucleus. (c) Grade II anulus. (d) Grade IV anulus. Facmu=500 in all cases.

did not agree. Thus this sample may be suspect (due to mis-grading or an undetected problem with the data collection that day) and the overlap between grades II and IV only occurs for sample 5. Sample 5 had the largest contributing component in the range above 100 ms, so the problem may originate with the arbitrary cut-off point of 20% for a "dominant" T_2 component.

Every sample had a short T_2 component with less than 20% contribution to the signal, regardless of grade, though the grade II samples have a consistent second small component between 15 and 40 ms that is only present in two of the grade IV samples. Table 6.3 lists the average T_2 values for grades II and IV, for the dominant components and the lesser components.

Table 6.3: **Average T_2 Values for Grades II and IV Anulus and Nucleus**

AF/NP	Grade	Contribution	# of Samples	Mean T_2 (ms)	Std. Dev. (ms)
NP	II	> 20%	5	138	49
NP	IV	> 20%	5	42	11
NP	II	shortest	5	4.7	1.5
NP	IV	shortest	5	4.5	2.6
AF	II	> 20%	3	23	6
AF	IV	> 20%	3	35	25

T_2 — Anulus Fibrosus: Unlike the nucleus samples, there was no significant difference between the dominant contributions to T_2 relaxation of grades II and IV, as seen in Figure 6.3 and Table 6.3. Due to this observation, further studies of the anulus fibrosus were discontinued in order to devote more time to the nucleus pulposus, where most change occurs with degeneration. The nucleus is also the region examined most closely in MRI grading procedures as it usually dominated the image.

As with the nucleus pulposus, all anulus samples had a short T_2 component of small amplitude, with the relaxation time falling between 1 and 5 ms. Generally, the

variation between samples is greater for grade IV than for grade II, though one must take into account the small number of samples when evaluating such trends.

T_1 — Nucleus Pulposus: The T_1 values follow a similar pattern to the T_2 results, with a large decrease from grade II to grade IV. Table 6.4 lists the average T_1 times for the dominant contributions to the spectrum; note the factor of two difference between grades. The division is clearer between grades than it is for T_2 , and no overlap occurs between the two groups.

The T_1 relaxation is simpler than the T_2 , having only one or two components in the spectra. This is expected for biological systems, as discussed in section 3.2.

Table 6.4: **Average T_1 Values for Grades II and IV Anulus and Nucleus**

AF/NP	Grade	Contribution	# of Samples	Mean T_1 (s)	Std. Dev. (s)
NP	II	> 20%	3	1.41	0.20
NP	IV	> 20%	3	0.74	0.10
NP	II	< 20%	2	0.44	0.26
NP	IV	< 20%	2	2.40	1.60
AF	II	> 20%	3	0.74	0.08
AF	IV	> 20%	3	0.86	0.21
AF	II	< 20%	2	1.35	0.07
AF	IV	< 20%	2	1.70	0.30

T_1 — Anulus Fibrosus: The T_1 values for the anulus are the same as those of the nucleus, except that the relative proportions of contributions to the spectrum are reversed: the dominant components have shorter T_1 values, and the small components have longer relaxation times. Table 6.4 shows the average T_1 values for large and small components of the spectra for grades II and IV disc anuli. Not all of the samples were found to have two components, or a large and small component — some had two contributions above 20%, for example.

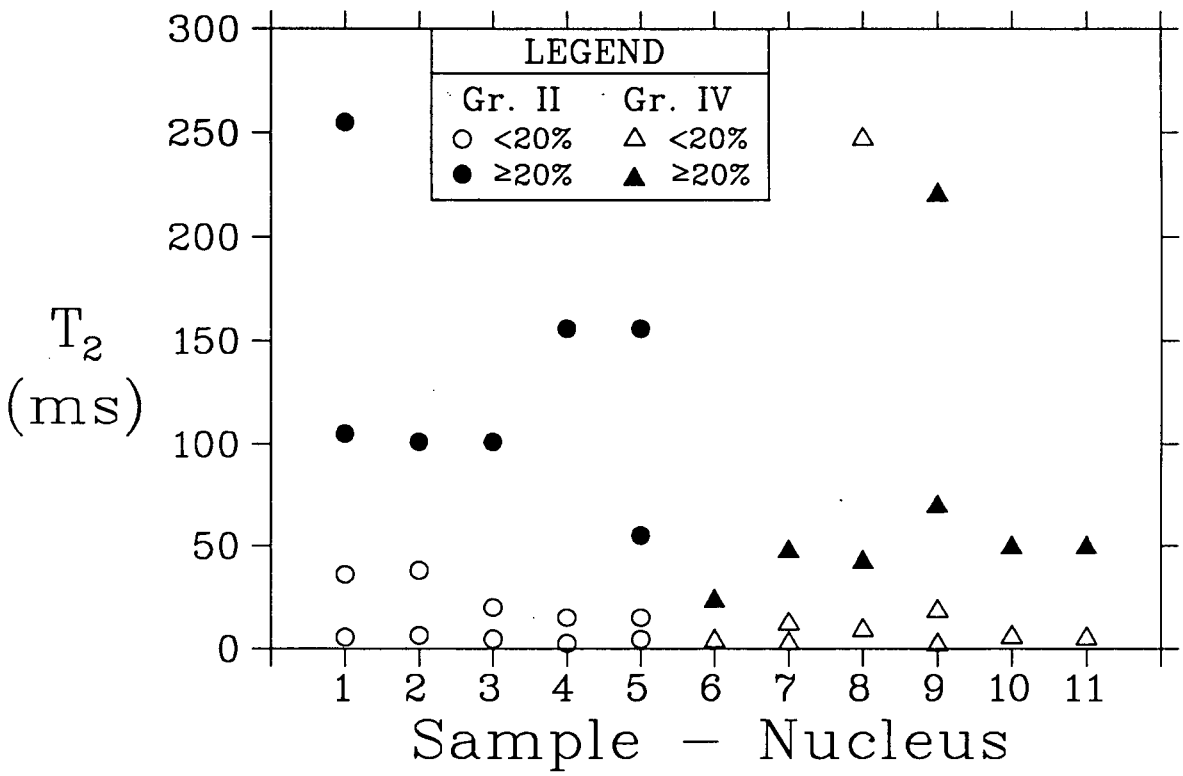

Figure 6.2: **Plots of T_2 values for in vitro disc nucleus samples.** Grade II and grade IV nucleus are displayed together (see legend). All components greater than or equal to 20% are shown as solid symbols, and the rest as empty symbols.

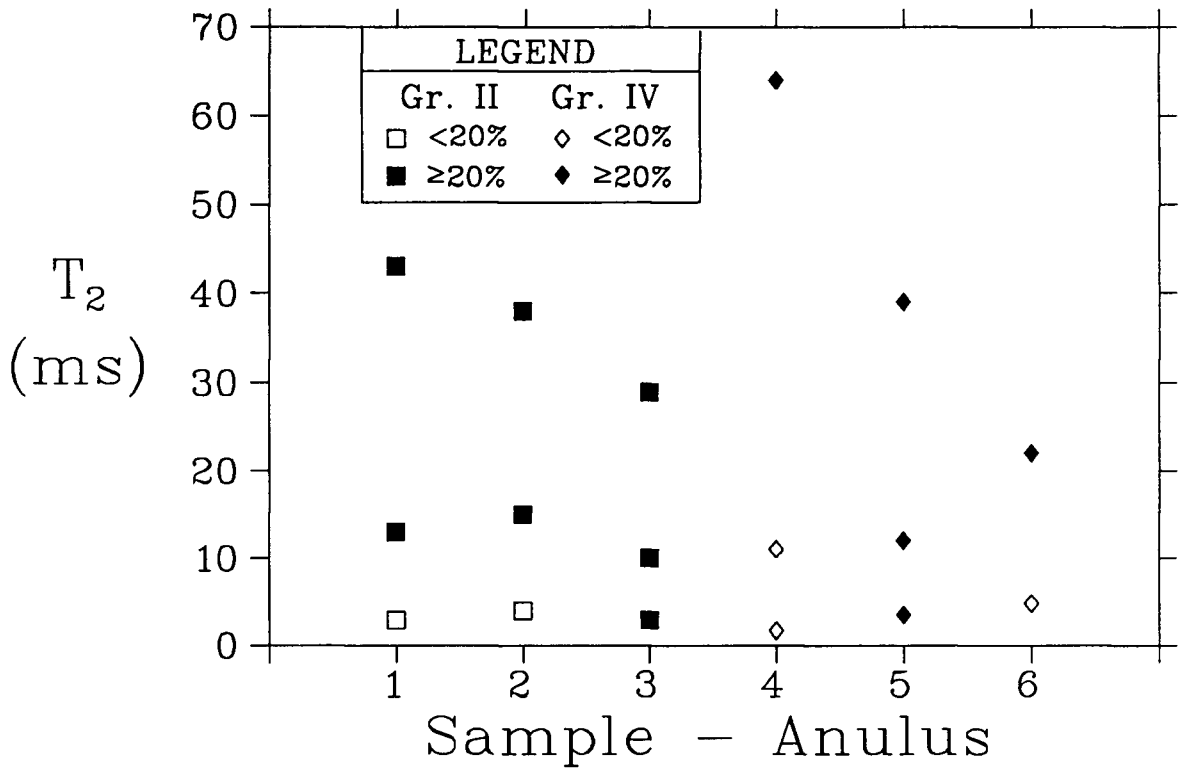

Figure 6.3: **Plots of T_2 values for in vitro disc anulus samples.** Grade II and grade IV anulus are displayed together (see legend). All components greater than or equal to 20% are shown as solid symbols, and the rest as empty symbols. Note that the vertical scale is much smaller than for the nucleus samples.

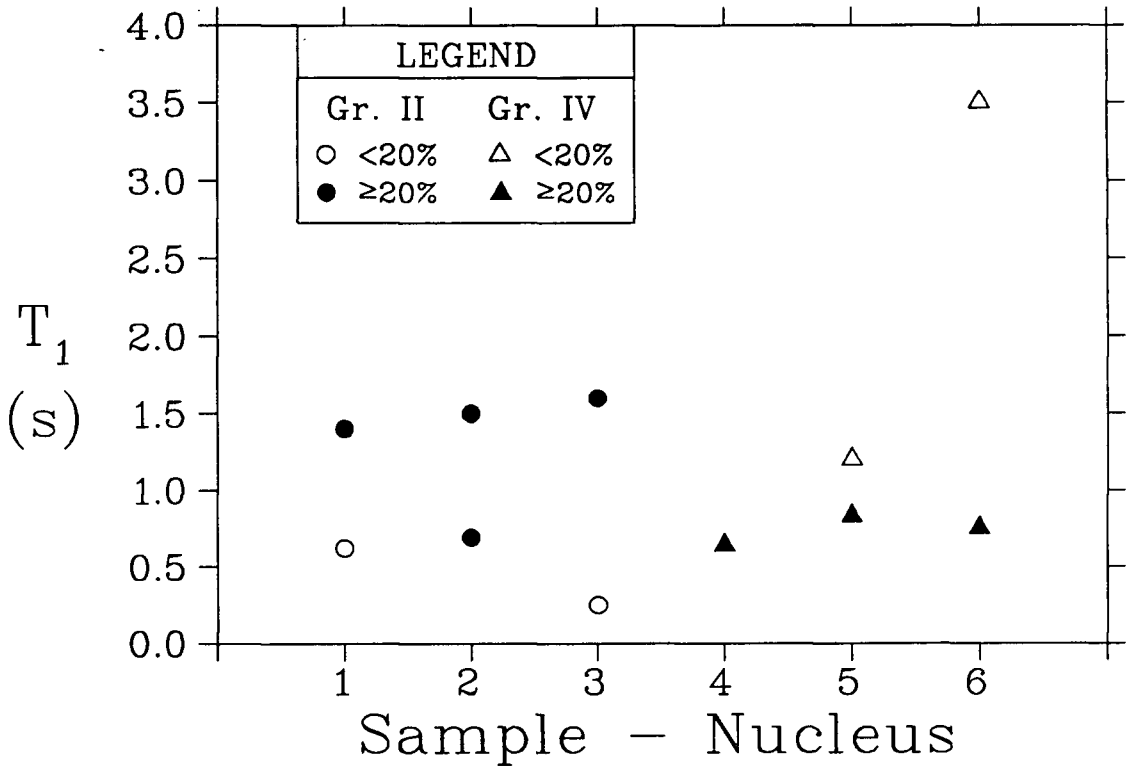

Figure 6.4: **Plots of T_1 values for in vitro disc nucleus samples.** Grades II and IV nucleus are displayed together (see legend). Symbols have the same meaning as in the corresponding T_2 plot.

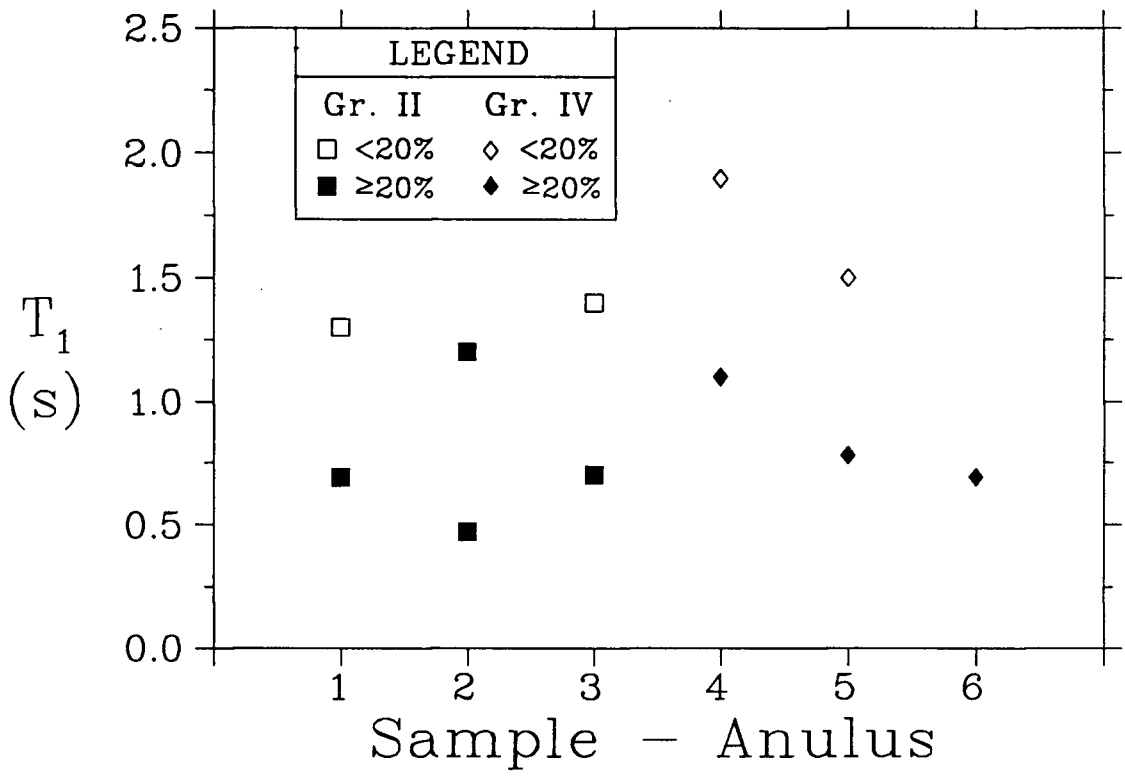

Figure 6.5: **Plots of T_1 values for in vitro disc anulus samples.** Grades II and IV anulus are displayed together (see legend). Symbols have the same meaning as in the corresponding T_2 plot. Note the scale difference from the nucleus T_1 plots.

Table 6.5: **T_2 Values (in ms) of In Vivo MRI Samples**

Volunteer #	Lumbar Disc Names:				
	L1–L2	L2–L3	L3–L4	L4–L5	L5–S1
1	134	131	126	110	143
2	43	50	57	44	27
3	90	90	81	40	83
4	118	120	56	35	47
5	128	108	129	148	57
6	25, 97	85	122	119	157
7	76	58	46	58, 181	86
8	44	44	49	52	57
9	94	151	51, 159	60	144
10	136	135	178	129	111
11	129	152	137	33, 168	41
12	93	40, 136	48	83, 255	68
13	124	124	131	35, 175	104
14	87	62, 234	65	78	49
15	69, 197	55, 139	62	55, 313	55, 147
16	93	36, 117	104	98	46
17	116	87	52	52	41
18	104	69	62	73	104
19	175	104, 395	117	35, 156	69

6.2 In Vivo MRI T_2 Values

All of the in vivo MRI T_2 values for the lumbar disc nuclei of the 19 volunteers studied are displayed in Table 6.5. In most cases where two components existed, they contributed fairly equally to the spectrum, so the actual percentages are not shown. Spectra were less complicated than those for in vitro samples because only twelve data points were available for fitting with the NNLS program.

Several of the volunteers were found to have self-consistent T_2 values among discs, such as volunteer #1 (average T_2 was 129 ms with a standard deviation of 12 ms), #2 (average 44 ms, standard deviation 11 ms), #8 (49 ms; 6 ms) and #13 (118 ms;

Table 6.6: **Average In Vivo T_2 Values for Each Lumbar Disc**

Disc:	L1–L2	L2–L3	L3–L4	L4–L5	L5–S1
Mean T_2 & Std. Error (ms)	104 ± 8	101 ± 8	91 ± 9	95 ± 10	81 ± 9

12 ms). This phenomenon can be seen in the first plot of Figure 6.6, which is a series of plots displaying all T_2 components found for each type of lumbar disc.

The mean T_2 values for each disc type are shown in Table 6.6. The weighted average T_2 values for two-component spectra were used in the calculations. Figure 6.7 provides a graphic illustration of those results, showing a trend towards shorter T_2 values from L1–L2 to L5–S1. The error bars represent the standard error of the mean and are slightly larger for the lower lumbar discs.

Figure 6.8 is a histogram plot of all the T_2 components found among the MRI volunteers, and shows clearly that there is a division of the values into two groups. The first group is centered around 50 ms, while the second is approximately centered on 120 ms. These numbers are not in disagreement with the average dominant T_2 values of in vitro nucleus samples found in Table 6.3.

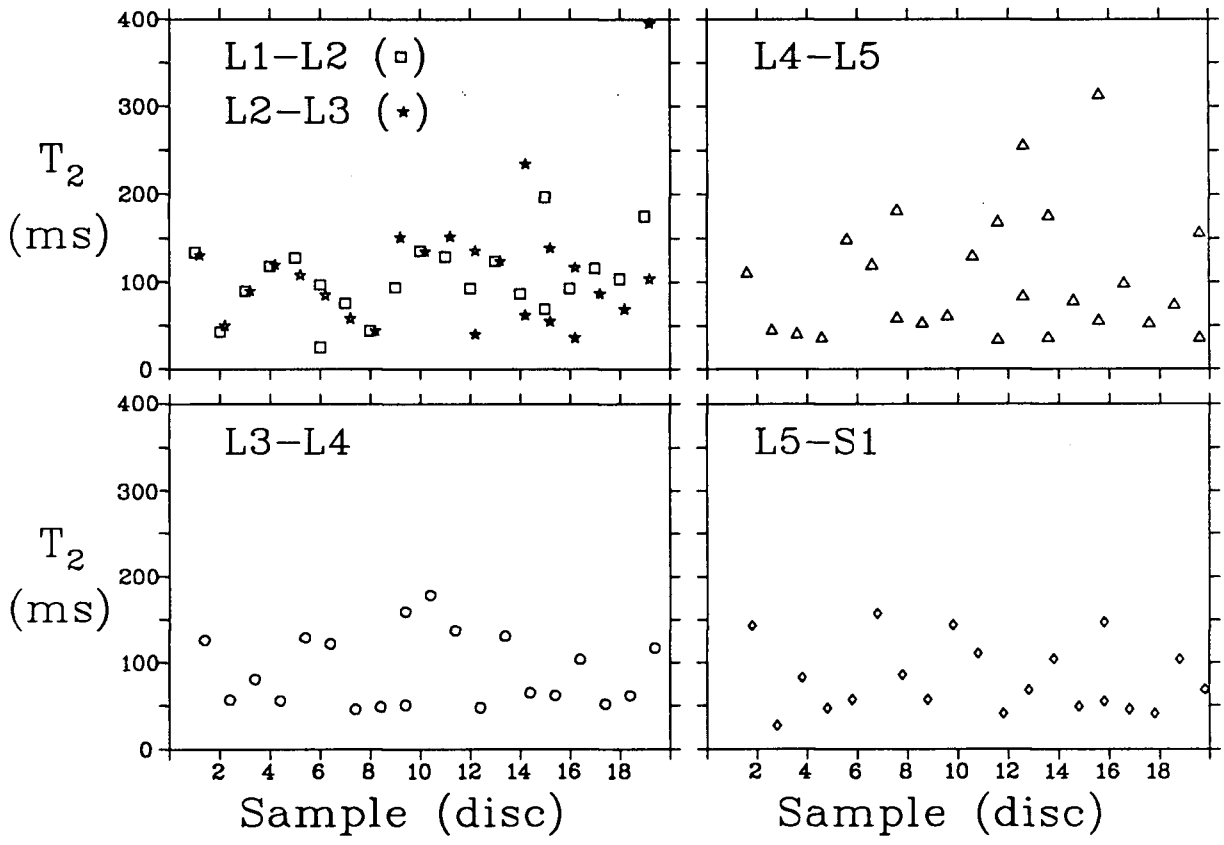

Figure 6.6: **T_2 values for MRI samples.**
Results for each disc are shown, with L1–L2 and L2–L3 overlaid to show similarity between discs of the same spine. The same vertical scale is used for all plots.

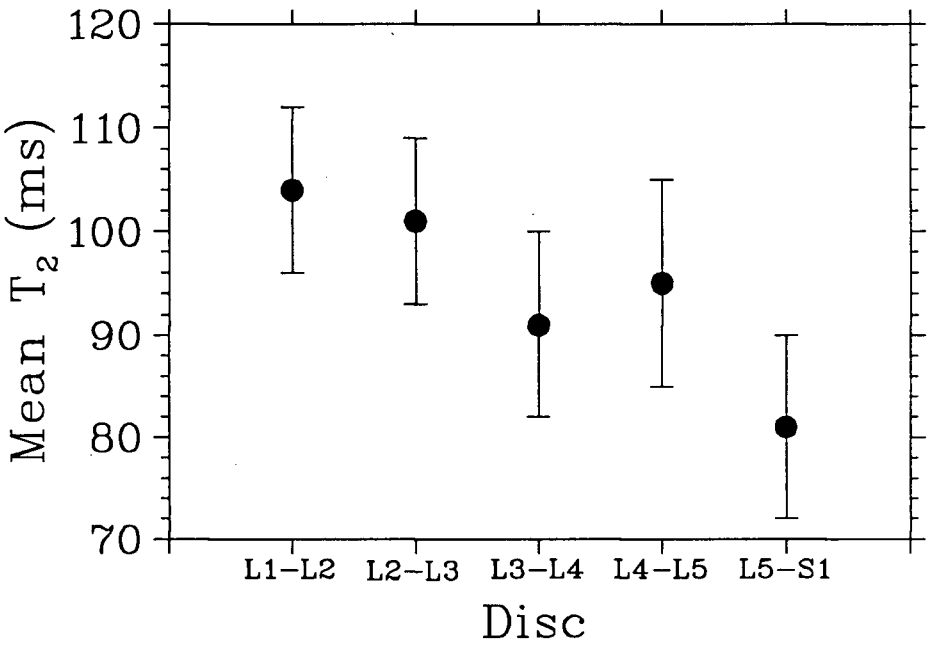

Figure 6.7: **Graph of mean MRI T_2 values for each disc.** This plot demonstrates the shortening of T_2 values from L1–L2 to L5–S1. Error bars represent the standard errors of the means.

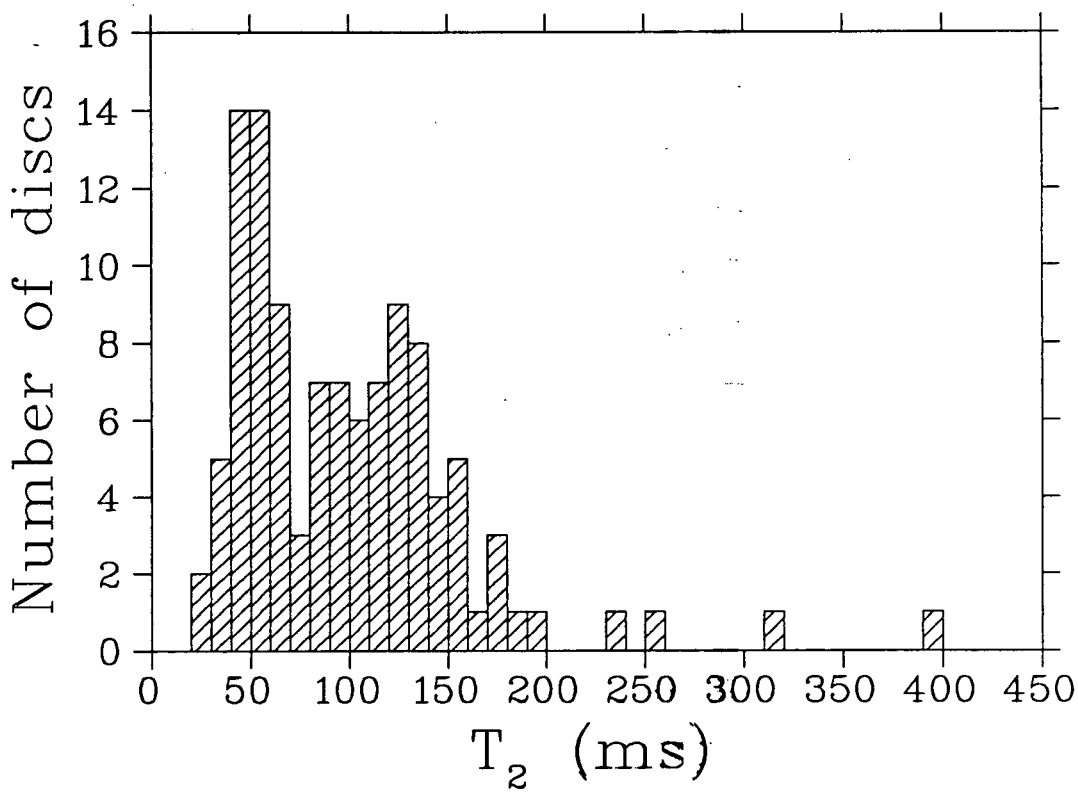

Figure 6.8: **Histogram of MRI T_2 values.**
All discs are included in this histogram, which demonstrates the grouping of T_2 values into two ranges.

6.3 Solid Signal in Disc Samples

The T_1 inversion-recovery data show the signal decay at times immediately after the 90° pulse. For very short tau values one may sometimes observe a rapidly relaxing component which can be attributed to protons of solids in the sample. Figure 6.9 shows inversion-recovery-data from samples of grade II and IV nucleus, with $\tau = 1$ ms. The grade II sample showed very little solid component (3.8%), while 8.5% of the signal from the grade IV sample was due to solid protons. This was calculated by separating the two decay slopes and interpolating back to $t = 0$. Although not shown, inversion-recovery data from anulus samples had a solid component making up 12% of the signal at $t = 0$, for both grades of disc.

6.4 T_1 and T_2 of Collagen Samples

Only one collagen sample from each of grades II and IV discs was examined, and these results are listed in Table 6.7. There did not appear to be any definite pattern to the relaxation times in this small sample group, but a few general observations were made. The T_1 values for the collagen were very similar for all samples (grades II and IV anulus and nucleus), but the grade IV samples had a longer T_1 component that was not present with the grade II samples. The T_1 values for grade II anulus and nucleus were identical. As far as T_2 went, the grade IV relaxation times were longer than those for grade II samples. A longer T_2 timescale was used for NNLS fits to accomodate the slow rate of relaxation.

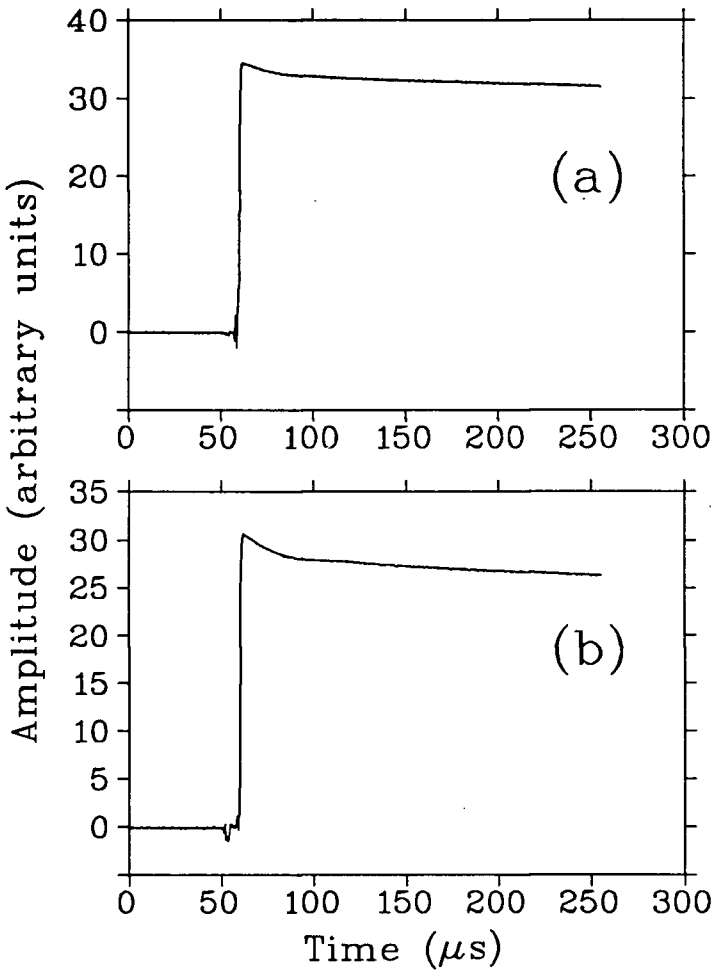

Figure 6.9: **Inversion-recovery data showing solid signal for in vitro disc samples.**
(a) Grade II nucleus pulposus. (b) Grade IV nucleus pulposus. The first 50μs is baseline. The solid portion of the signal shows up as the steeper slope immediately after the pulse.

Table 6.7: **T_1 and T_2 Values for Collagen Samples**

Sample	AF/NP	Grade	T_1 Values (s) and % Contributions	T_2 Values (ms) and % Contributions
C1N	NP	II	1.5 (100%)	76 (37%) 183 (63%)
C2N	NP	IV	1.3 (81%) 3.1 (19%)	327 (100%)
C1A	AF	II	1.5 (100%)	9 (1%) 99 (99%)
C2A	AF	IV	1.0 (64%) 2.1 (36%)	80 (72%) 1180 (28%)

6.5 T_1 and T_2 of Proteoglycan Samples

Both T_1 and T_2 relaxation for proteoglycan samples in saline were single or almost single exponential. Table 6.8 lists the relaxation times. As proteoglycan concentration decreased, relaxation times increased for both anulus and nucleus proteoglycan, with the T_1 and T_2 values shorter for anulus than nucleus at similar concentrations. Figure 6.10 illustrates the changes of relaxation *rates* with proteoglycan concentration; the relationship is roughly linear for the three concentrations studied. In all cases, the T_2 values are much longer than those of the disc samples.

Table 6.8: **T_1 and T_2 Values for Proteoglycan Samples**

Sample	AF/NP	Concentration (mg/ml)	T_1 (s)	T_2 (ms)
PGN1	NP	155.3	2.00	666
PGN2	NP	74.0	2.42	1100
PGN3	NP	49.8	3.20	1340
PGA1	AF	143.6	1.42	440
PGA2	AF	71.6	1.74	666
PGA3	AF	50.1	—	750

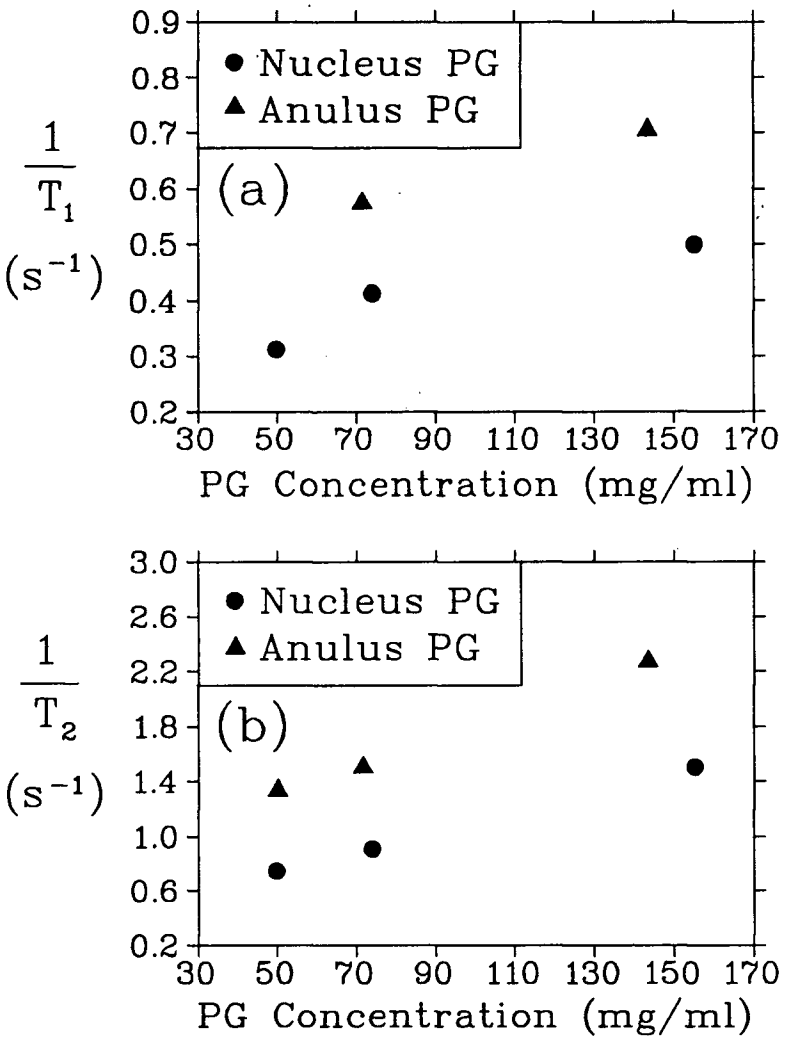

Figure 6.10: **Graphs of proteoglycan relaxation rates versus concentration in saline solution.**
(a) $1/T_1$ versus concentration for anulus and nucleus PG.
(b) $1/T_2$ versus concentration for anulus and nucleus PG.

Chapter 7

Discussion

Correlation of relaxation times with grade: The results of the in vitro disc studies show that relaxation times correlate with disc grade. T_2 and T_1 values of the nucleus change significantly with grade, decreasing by approximately a factor of two between grades II and IV. Furthermore, the MRI T_2 values decrease with distance down the lumbar spine, which would be expected if T_2 were inversely proportional to disc grade: the lower discs of the lumbar region are generally the most degenerate. Another fact supporting the notion that T_2 is a sensitive indicator of degeneration is that the results for the grade IV nucleus look the same as those of both grades of anulus. This ties in with the fact that as discs degenerate, the nucleus becomes more and more like the anulus until they are indistinguishable, as noted in Section 2.2.

Comparison of in vitro and in vivo relaxation times: The in vivo T_2 values agree with those found in vitro, being grouped into two ranges of relaxation times that match the grades II and IV in vitro T_2 values. These results agree despite the differences in sample temperature and NMR frequency during data collection. The in vitro sample data were collected at approximately 23°C while the in vivo samples remained at 37°C. An increased temperature would be associated with faster thermally activated processes and increased diffusion rates. Correlation times decrease with increased thermal activity, but this should not affect T_2 unless slow motions are present. The lack of dependence of T_2 on CPMG tau value suggests that slow motions do not play a large

role in relaxation. The change in diffusion rate would shorten T_2 if the relaxation were diffusion-limited, but here that does not seem to be the case, as the T_2 times agree for room temperature and body temperature. As for frequency differences, the in vitro experiments were carried out at 90 MHz, while the MRI data were collected at 6.4 MHz. This would not be expected to affect T_2 values since the fundamental mechanism for transverse relaxation is dipole-dipole, which is independent of field strength. T_1 on the other hand should be much shorter at the MRI frequencies compared to 90 MHz, and this is the case: the shortest in vitro T_1 value is 740 ms, while in vivo values are typically 370 ms [19].

Distribution of in vivo T_2 values: The two peaks in the distribution of in vivo relaxation times are relatively wide (Figure 6.8, indicating the disparity among individuals' T_2 values. Separate consideration of the data for each subject suggests that relative, not absolute, evaluations of T_2 data would be most useful from a clinical point of view — often one disc in a spine will have a much lower T_2 value than any of the others, while another spine will have these "low" T_2 values for every disc, even though no other evidence of degeneration appears. For an example of this, compare samples 5 and 8 in Table 6.5. The L5–S1 disc of sample 5 has a T_2 value of 57 ms which is half as long as the values for the other discs, yet the discs of sample 8 all have T_2 values equal to or lower than 57 ms.

Proteoglycan and collagen studies: The changes in T_2 with grade are probably related more to structure than to chemical composition, as noted in section 4.1. The results of the proteoglycan studies support this theory: though proteoglycan appears to be lost from the disc during degeneration, simply decreasing the concentration of isolated proteoglycan does not decrease the T_2 value; rather, it increases, contrary to

the behaviour in discs when pg content is lowered. This is not unexpected, however, because when less proteoglycan is in solution, the water behaves more like bulk water, and the T_2 times should increase. These results are in agreement with a recent study by Weidenbaum et. al [20]. Collagen studies also demonstrate this contradictory behaviour, with T_2 values being longer for grade IV collagen extract than for grade II. As suspected, studies of these macromolecules in isolation cannot be directly applied to disc studies. Instead, one must consider the structure of the cartilage as a whole. If proteoglycan aggregates and their subspecies are fragmenting with degeneration, this may shorten T_2 by reducing the volume of bulk water between molecules, i.e. decreasing the mean diffusion path for a water molecule. The decreasing water content would add to this effect. In addition, collagen increases in the nucleus with degeneration, reducing bulk water and increasing the amount of structured water.

Details of T_2 spectra: The components of the T_2 spectra are at different T_2 values for grades II and IV, rather than having peaks at the same T_2 values with different relative contributions to the total area. This rules out a simple model of compartments relaxing separately, with relative volumes changing during degeneration. The only common component of the spectrum is the very short (less than 10 ms) T_2 peak, which contributes about 5%.

The following calculation roughly estimates the percentages of protons in the water, proteoglycan and collagen of the grade II nucleus, for comparison with the components of the T_2 spectra. First of all, the healthy disc is about 70% water. Collagen makes up 10–20% of the dry weight in the nucleus (Section 2.2), so the remaining 80–90% would be proteoglycan. This means that of the total wet weight, there would be about 70% water, 4.5% collagen, and 25.5% proteoglycan. Water has 2 protons per 18 atomic units, or 0.11 protons per unit weight. Rough estimates of the number of protons

per unit weight for the proteoglycan and collagen are 0.12 and 0.067, respectively. So, multiplying these fractions by the weight percentages of water, pg and collagen in the nucleus gives the following percentages of protons: 78% from water, 17% from proteoglycan, and 5% from collagen. For a grade IV nucleus, the percentage from water would decrease, as water content drops by 30%; the percentage from proteoglycan would be increased by water loss and decreased due to proteoglycan loss; and the percentage from collagen would increase both from decreased water content and increased collagen content.

The solid component of the spectrum as shown in Figure 6.9 accounts for 3–4% of the signal in the grade II nucleus, so it seems likely to originate from the protons of the collagen. This theory is supported by two results: the solid component increases to 8–10% in grade IV nucleus, and collagen is known to increase with degeneration; also, the solid signal in the anulus was the largest at 12%, which also agrees with the known chemistry of the disc. Further evidence comes from the slope of the solid signal, which increases from grade II to grade IV, suggesting a more rigid structure is responsible for the signal; collagen fibrils are known to increase in diameter with degeneration.

The shortest T_2 component in the grade II and grade IV nucleus spectra contributes 1–7% and thus could be attributed to bound water or proteoglycan, with cross-relaxation possibly playing a role. The second short component in the grade II nucleus spectra ranges from 4–15% contribution, with T_2 values from 15 to 38 ms, and this might be due to the protons of the proteoglycan, which are estimated at 17% abundance. The large components of the grade II spectra most likely originate from the bulk and hydration water. For the grade IV nucleus, the largest component of the spectra has T_2 values in the range 23–50 ms and no third T_2 component, so it appears that for grade IV, the proteoglycan and bulk water protons are indistinguishable in terms of T_2 values. Table 7.1 lists tentative assignments of all components of the T_2

Table 7.1: **Tentative Assigments to the T_2 Spectrum for Disc Nucleus**

Constituent	Assignment	Grade II Proportion of Protons	Grade IV Proportion of Protons
Collagen	T_2^*, 20–40μs (solid signal)	3–4%	8–10%
Bound water or proteoglycan	T_2, 1–6 ms	1–5%	2–7%
Proteoglycan or water	T_2, 15–50 ms	4–14%	82–89%
Water	T_2, >100 ms	48–92%	—
		Total=100%, including solid	

spectra for the disc nucleus, grades II and IV. Cross-relaxation between some or all of these constituents is probable and leaves several models open for investigation.

Details of T_1 spectra: The T_1 spectra differ from the T_2 spectra in that they *do* have common values that occur in different relative contributions. Different processes seem to be at work for T_1 relaxation, probably because cross-relaxation processes would have more time to act on a T_1 timescale. The large difference between T_1 and T_2 indicates that fast motions with correlation times less than 1/90 MHz are of importance to the relaxation processes. The complex T_2 spectra are probably more useful for studying details of the degenerative mechanism, though the T_1 results are necessary to complete the picture.

Future work: More accurate assignment of the components of the T_2 spectrum to specific molecules and processes in the disc will require further experiments with in vitro and in vivo disc samples. First of all, more disc samples should be measured, both in vitro and in vivo, to gain a larger sample of the population from which robust statistics can be extracted. As well, the same samples should undergo chemical analysis

so that the exact amounts of water, proteoglycan and collagen are known for each sample. This would allow precise comparisons between chemistry and NMR data, and contrast between samples of different grades. Histological analysis would also be valuable in correlating disc structure with the T_1 and T_2 results. Meanwhile, in vitro data collection should be attempted at 37°C on samples that have not been previously frozen, to eliminate the possibility of structural differences between in vivo and in vitro tissues.

Conclusions: This study has formed the framework for continuing research regarding the application of magnetic resonance to the intervertebral disc. The results of this investigation indicate that relaxation measurements, in particular T_2, are sensitive to disc degeneration and could be used as the main tool for studying the details of the degenerative mechanism. The T_1 and T_2 spectra, the in vivo T_2 values, and the solid signal measurements strongly support the suggested roles of collagen, proteoglycan and water in NMR measurements of the intervertebral disc. Future work will be based on verifying and expanding the model proposed here.

Bibliography

[1] R. H. Pearce, J. P. Thompson, B. Flak, A. MacKay. "Biochemical and Radiologic Studies of Degeneration in the Human Intervertebral Disc". A research proposal to the Arthritis Society, December 1989.

[2] M. T. Modic in Magnetic Resonance Imaging of the Spine. Chapter 3: "Degenerative Disorders of the Spine", pp75–119. Yearbook Medical Publishers, Chicago, London, Boca Raton, 1989.

[3] D. Eyre, P. Benya, J. Buckwalter, B. Caterson, D. Heinegard, T. Oegema, R. Pearce, M. Pope, J. Urban. New Perspectives on Low Back Pain. Part B: Basic Science Perspectives. Eds. J. W. Frymoyer, S. L. Gordon. Park Ridge, IL. American Academy of Orthopaedic Surgeons, pp147–207, 1989.

[4] R. H. Pearce, B. J. Grimmer, M. E. Adams. "Degeneration and the Chemical Composition of the Human Lumbar Intervertebral Disc". *J. Orth. Research*, **5**:198–205, 1987.

[5] A. I. Caplan. "Cartilage". *Sci. Am.*, **251**:84–94, 1984.

[6] E. D. Harris, Jr. Scientific Bases of Rheumatology Chapter 16: "Biology of the Joint." (Futher information unavailable)

[7] J. J. DiFabio, R. H. Pearce, B. Caterson, H. Hughes. *Biochem. J.*, **224**:27–33, 1987.

[8] R. H. Pearce, B. J. Grimmer. "The Concentration of Proteoglycan Fractions in Healthy Young Human Lumbar Intervertebral Discs". Preprint, 1989.

[9] G. M. Bebault, R. H. Pearce. "The Assay of Keratan Sulfate as Anion-Exchanger-Bound Hexose". Preprint, October 1989.

[10] J. P. Thompson. "Classifications of Gross Morphologic and Magnetic Resonance Images of Human Intervertebral Discs". M.Sc. Thesis, UBC, 1987.

[11] J. P. Thompson, R. H. Pearce, M. T. Schechter, M. E. Adams, I. K. Y. Tsang, P. B. Bishop. "Preliminary Evaluation of a Scheme for Grading the Gross Morphology of the Human Intervertebral Disc". Submitted to *Spine*, October 1989.

[12] C. P. Slichter. Principles of Magnetic Resonance pp1–42. Springer-Verlag, Berlin, Heidelberg, New York, 1980.

[13] R. Mathur-De Vre. "The NMR Studies of Water in Biological Systems" *Proc. Biophys. Mol. Biol.*, **35**:103–134, 1979.

[14] P. S. Belton, R. G. Ratcliffe. "NMR and compartmentation in Biological Tissues" *Progress in NMR Spectroscopy*, **17**:241–279, 1985.

[15] G. D. Fullerton in Magnetic Resonance Imaging. Chapter 3: "Physiologic Basis of Magnetic Relaxation", pp36–55. C. V. Mosby Company, St. Louis, Washington, D. C. Toronto, 1988.

[16] K. R. Brownstein, C. E. Tarr. "Importance of classical diffusion in NMR studies of water in biological cells" *Phys. Rev. A.*, **19**:2446–2453, 1979.

[17] E. Sternin. Ph.D Thesis, UBC, 1988. pp34–45.

[18] K. P. Whittall, A. L. MacKay. *J. Magn. Resonance*, **84**:64, 1989.

[19] A. MacKay, private communication.

[20] M. Weidenbaum, R. J. Foster, B. A. Best, E. L. Nickoloff, A. Ratcliffe, R. Jelsma, J. H. Newhouse, V. C. Mow. "Magnetic resonance imaging studies of water and proteoglycan content of the intervertebral disc". p338, 36th Annual Meeting, Orthopaedic Research Society, New Orleans, Louisiana, February 5–8, 1990.